A Significant Tornado Event near a Dryline Bulge in Northern Italy

FRANCESCO DE MARTIN,[a,b] FEDERICO PAVAN,[b] NICOLA CARLON,[b,c] GUIDO CIONI,[d] CHRISTOPHER ROZOFF,[e] VIRGINIA POLI,[f,g] SEBASTIANO CARPENTARI,[b,h] AND MARIO MARCELLO MIGLIETTA[i]

[a] *Department of Physics and Astronomy, Alma Mater Studiorum–University of Bologna, Bologna, Italy*
[b] *PRETEMP, Pordenone, Italy*
[c] *Radarmeteo, Due Carrare, Italy*
[d] *Meteonetwork, Milan, Italy*
[e] *U.S. National Science Foundation, National Center of Atmospheric Research, Boulder, Colorado*
[f] *Hydro-Meteo-Climate Structure,Regional Agency for Prevention, Environment and Energy of Emilia-Romagna, Bologna, Italy*
[g] *ItaliaMeteo Agency, Bologna, Italy*
[h] *Department of Civil, Environmental and Mechanical Engineering, University of Trento, Trento, Italy*
[i] *Institute of Atmospheric Sciences and Climate (CNR-ISAC), National Research Council of Italy, Padua, Italy*

(Manuscript received 6 April 2025, in final form 12 July 2025, accepted 22 July 2025)

ABSTRACT: A multiscale observational analysis of a 1.5-km-wide IF3 (International Fujita scale) tornado in northern Italy is conducted using radar and sounding data, ground weather stations, and damage surveys. The tornado occurred close to Alfonsine, along the Adriatic coast, on 22 July 2023, in one of the most tornado-prone regions of Europe. An initially hail-bearing supercell (which produced hailstones up to 10 cm in diameter) became tornadic as it approached a dryline bulge and a maritime air mass with very high-Θ_e values. Before the tornadogenesis occurrence, the supercell significantly turned right and generated a damaging rear-flank downdraft (RFD) surge, with unusually cold wind gusts reaching 40 m s^{-1}. A dry and hot air mass from the southwest was partially ingested by the mesocyclone just before the tornado developed. A seamless wind damage pattern, transitioning from damage caused by straight-line wind gusts to tornadic damage, suggests that the tornado may have developed from the stretching of small-scale pretornadic vertical vorticity maxima within the RFD. Numerical simulations indicate that the long-lived supercell was predictable since they consistently simulated updraft helicity tracks in the area for 3 consecutive days ahead of the event. The tornado resulted in only 14 injuries, likely because it impacted a sparsely populated area. Considering that past significant tornadoes in the region affected much more densely populated areas, and since no tornado warnings or shelters are currently in place, there are growing concerns about the potential catastrophic consequences of a future significant tornado in northeastern Italy.

SIGNIFICANCE STATEMENT: A multiscale observational analysis of a wide IF3 (International Fujita scale) tornado in northeastern Italy, a significant tornado hotspot in Europe, is conducted. An initially hail-bearing supercell became tornadic as it approached a very moist maritime air mass. The long-lived supercell was predictable up to 3 days in advance and maintained a consistent trajectory, suggesting that a tornado outlook and warning could have been issued. However, Italy remains unprepared to face a major tornado event. Residents in the most affected areas should be educated about tornado risks, tornado outlooks should be issued by Italian Civil Protection, a nowcasting-based tornado warning system should be implemented, and shelters should be built in specific settings (e.g., outdoor event venues, beaches, and sports facilities).

KEYWORDS: Complex terrain; Europe; Drylines; Tornadoes; Surface observations; Damage assessment

1. Introduction

Research on tornadoes in Europe is less advanced and extensive than in the United States, primarily because tornadoes are much more frequent in the latter (Taszarek et al. 2020a). However, tornado risk in Europe is not negligible and is significantly higher than most Europeans perceive (Doswell 2003). Over the past two decades, European researchers have made considerable efforts to bridge the gap with the United States by conducting numerous studies. Both national (e.g., Miglietta and Matsangouras 2018 for Italy, Matsangouras et al. 2014 for Greece, and Taszarek and Brooks 2015 for Poland) and continental-scale (Groenemeijer and Kühne 2014; Dotzek 2003) climatologies of tornadoes have been developed. These studies have identified northern Italy, particularly its eastern part, as one of the most significant tornado hotspots in Europe. Environmental precursors of European tornadoes have been investigated using both sounding data (Taszarek et al. 2017; Púčik et al. 2015; Groenemeijer and van Delden 2007) and reanalysis datasets (Bagaglini et al. 2021; Taszarek et al. 2020b; Ingrosso et al. 2020; Coffer et al. 2020; Romero et al. 2007).

Denotes content that is immediately available upon publication as open access.

Supplemental information related to this paper is available at the Journals Online website: https://doi.org/10.1175/WAF-D-25-0071.s1.

Corresponding author: Francesco De Martin, francesco.demartin2@unibo.it

DOI: 10.1175/WAF-D-25-0071.1

These studies highlight notable differences between tornado environments in the United States and Europe, with European tornadoes generally occurring in environments with much lower latent instability. Additionally, several high-resolution numerical simulations of tornado case studies across the continent have been conducted to examine mesoscale environments (e.g., Pilguj et al. 2022; Avolio and Miglietta 2022), assess predictability (e.g., Antonescu et al. 2020), and investigate the role of local topography (e.g., Miglietta et al. 2017; Homar et al. 2003).

Detailed damage surveys are sometimes conducted in Europe, though not as systematically as in the United States (Horton 2024; Holzer et al. 2018; Wesolek and Mahieu 2011; Lemon et al. 2003). In Italy, damage surveys for some significant tornadoes have been conducted, although they are generally not published in peer-reviewed journals (e.g., Longo and Puppo 1934; Janeselli 1972; ESSL 2015), with the exception of the F4 tornado in Mira–Dolo on 8 July 2015 (Zanini et al. 2017). Damage surveys across Europe highlight limitations in applying the Fujita and enhanced Fujita (EF) scales to European buildings (e.g., Chmielewski et al. 2013; Zanini et al. 2017). To address these issues, the European Severe Storm Laboratory (ESSL) introduced the International Fujita (IF) scale to rate wind damage from both straight-line winds and tornadoes (Groenemeijer et al. 2023). The IF scale differs from the EF scale the way damage indicators (DIs) and degree of damage are identified and evaluated, as well as in how wind speeds are estimated. While the EF scale estimates 3-s gusts, the IF scale estimates instantaneous three-dimensional wind speeds. Púčik et al. (2024) recently applied this scale for the first time to an IF4 tornado that struck Czechia on 24 June 2023, where a highly detailed damage survey was conducted in the days following the event.

One aspect still poorly addressed in the scientific literature on European tornadoes is the analysis of ground and radar observations of tornadic supercells, probably due to the limited coverage and quality of radar data, although the situation has improved in the last few years. Notable exceptions include Bech et al. (2007, 2011) in Catalonia, who studied a tornado outbreak in 2005 and an F2 tornado in 2008, respectively, with a strong focus on radar observations. A few additional observational studies, primarily based on radar data, were conducted in Germany (Hannesen et al. 2000) and Czechia (Komjáti et al. 2022). In Italy, some observational studies based on ground weather stations and radar data were conducted in the northeastern region (Bertato et al. 2003; Bechini et al. 2001; Giaiotti and Stel 2007). Recently, De Martin et al. (2024) proposed a conceptual model for tornado development in the Po Valley, integrating ground and radar observations with numerical simulations. They suggested that tornadoes in the Po Valley typically occur near a triple point, where surface boundaries enhance latent instability and low-level wind shear. However, the number of observational studies of major tornado events in Europe remains significantly lower than in the United States, where extensive field campaigns were carried out.

The lack of observational studies on tornadic supercells is a major limitation in understanding tornado environments in Europe. Field campaigns in the United States have led to substantial advancements in tornadogenesis research by confirming or refuting theoretical and numerical hypotheses (Rotunno and Bluestein 2024). Similar observational campaigns would be particularly beneficial in Europe because mesoscale features play such a prominent role in severe convective weather here (Scheffknecht et al. 2017; Miglietta et al. 2016). The upcoming Thunderstorm Intensification from Mountains to Plains (TIM) campaign may help to fill this gap (Fischer et al. 2025).

Last, tornado predictability and warning systems are critical issues in Europe. The need for a dedicated early warning system for tornadoes has been emphasized multiple times over the past two decades (Antonescu et al. 2017; Miglietta and Rotunno 2016; Doswell 2003). However, only a few European countries issue specific tornado warnings (Rauhala and Schultz 2009), and Italy is not among them, despite being one of the most tornado-prone countries on the continent. The absence of tornado warnings in Europe is often justified by the relatively low frequency of these events, which is deemed insufficient to warrant a dedicated warning system. However, Antonescu et al. (2017) highlighted the substantial number of injuries, fatalities, and economic losses caused by tornadoes in Europe, despite their relative rarity. The recent sinking of the "Bayesian" yacht in Sicily on 19 August 2024, which led to seven fatalities and was caused by a nocturnal local severe storm, further emphasizes Europe's vulnerability to convective winds (De Martin et al. 2025b).

Another argument against tornado warnings in Europe is the perceived low predictability of these events. This concern is partly valid, as European tornado environments are less well understood than those in the United States (due to the lack of observational studies) and because the complex morphology of northern Italy reduces the predictability of supercells (e.g., Pilguj et al. 2022; Miglietta et al. 2016 showed that numerical simulations struggle to properly simulate severe storms in the complex topography of northern Italy). However, reliable tornado forecasting is possible in Europe, at least in the flat plains of central Europe: Antonescu et al. (2020) demonstrated that the tornado outbreak affecting France, the Netherlands, and Belgium on 25 June 1967 would have been predictable using modern numerical models.

This study aims to contribute to filling these gaps in European tornado research by investigating the remarkable tornado that struck Alfonsine (Fig. 1) in northern Italy on 22 July 2023. This tornado caused 14 injuries and no fatalities, which are relatively low numbers compared to other tornadoes in the region (e.g., the Mira–Dolo tornado in 2015 caused 72 injuries and 1 fatality; ESSL 2015). This event is particularly intriguing because no footage or photos of the vortex are available, and initially, there were suspicions that it was a strong microburst event instead of a tornado. As a result, multiple surveys were carried out by weather enthusiasts ("Meteo 5.0") and experts from the "Emilia Romagna Meteo" organization to analyze the damage pattern. Moreover, the affected area is covered by a dense network of ground weather stations, with a sounding and radar site located just 30 km to the west. Additionally, operational numerical model output is available to further study the mesoscale environment and to assess the predictability of the tornadic supercell. Thus, this event inspires the following questions: (i) Does the conceptual model of De Martin et al. (2024) apply to the present event? (ii) Was the tornadic supercell predictable?

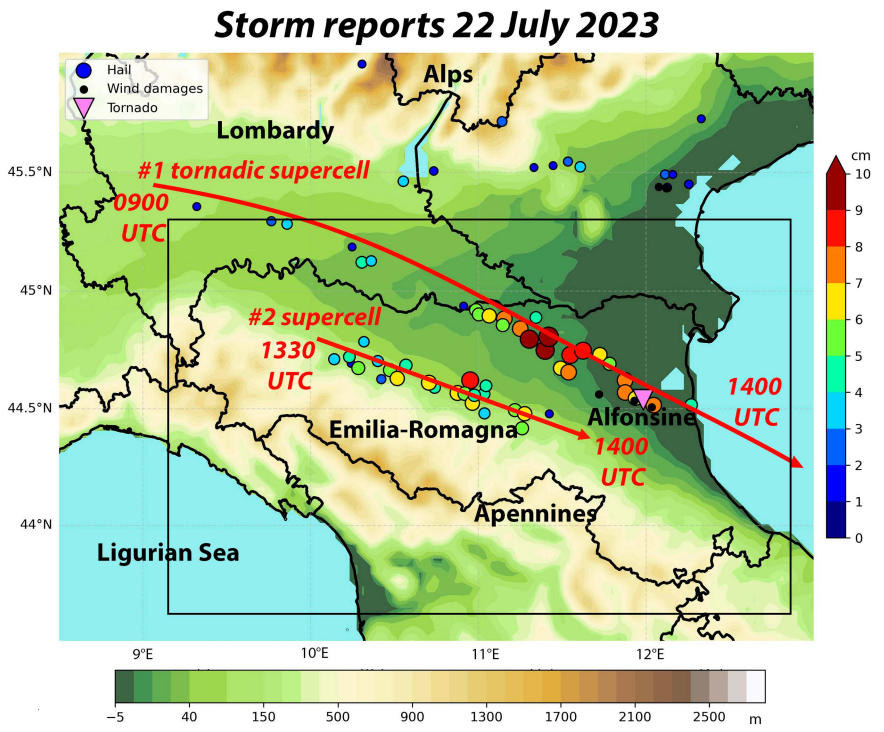

FIG. 1. Topography of northern Italy (scale in the bottom) and relevant locations mentioned in the text are shown. Hail reports (filled colored dots; hail size according to the scale on the right), wind damage report (black dots), and tornado (purple triangle) are displayed. The two red arrows emphasize the paths of storms 1 and 2, with starting and ending times. The box highlights the domain shown in Fig. 3.

(iii) Was this area prepared to face a major tornado event? (iv) What insights does this event suggest regarding exposure and vulnerability to tornado risk?

In section 2, the methods and data used in the manuscript are described. In section 3, the synoptic and mesoscale situation are analyzed, along with radar images and data from ground weather stations. The results from the damage surveys, a numerical simulation, and the predictability of the event are analyzed as well. In section 4, the dynamics of the tornadic supercell is summarized, and the exposure and vulnerability to the tornado risk in this region are discussed. Answers to the aforementioned questions will be provided. Finally, in section 5, conclusions are drawn, and suggestions regarding how to handle tornado risk in this area will be given.

2. Methods and data

a. *Meteorological data*

We use ERA5 reanalysis to assess the synoptic environment of the event (Hersbach et al. 2020). The vertical properties of the atmosphere just before the tornado occurrence are obtained from the sounding launched in San Pietro Capofiume (WMO 16144, location shown with a black dot in Fig. 3a) at 1100 UTC 22 July 2023. Instability and kinematic sounding-derived parameters are computed using the ThundeR software (Czernecki et al. 2022).[1] Ground weather station data managed by the Meteonetwork association, which are subject to quality control (Giazzi et al. 2022), are used to study the prestorm mesoscale environment. Three weather stations of the Weather Underground network located close to the tornado path are used as well. Their data are compared to the ones of the Meteonetwork association to qualitatively assess their reliability during the event. In the supplemental animation Video S1 the surface rainfall intensity (SRI) provided every 5 min by the national composite radar network managed by the Civil Protection Department of Italy with 1-km grid spacing is plotted with Meteonetwork weather station data. The weather stations are also helpful to identify the presence of the mesocyclone and the outflows of supercell 1. The perturbed values of virtual potential temperature Θ_v' and pressure p', obtained by subtracting from the instantaneous value the time mean in the 2 h before the storm passage, were used as proxies for the downdraft and the mesocyclone, respectively, as commonly done in tornado studies (e.g., Markowski et al. 2002).

Radar reflectivity measured by the C-band radar of San Pietro Capofiume (the same location of the sounding, shown with a black dot in Fig. 3a) is used to study the supercell features. Radial velocities were too noisy to be used.

[1] An explanation of the plotted parameters is available at http://www.rawinsonde.com/thunder_app/thundeR_v1_1_parameters.pdf.

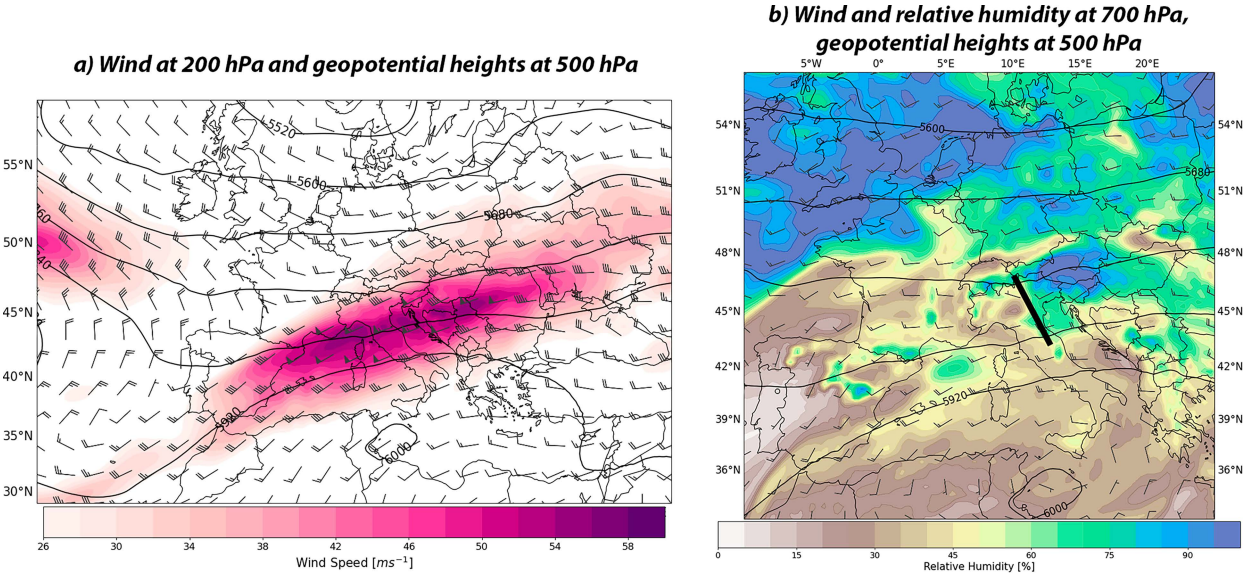

FIG. 2. ERA5 reanalysis data at 1200 UTC 22 Jul 2023: (a) wind at 200 hPa (barbs and color shading) and geopotential heights (gpm; contours) at 500 hPa; (b) wind (barbs) and relative humidity (color shading) at 700 hPa. A half barb is 5 m s^{-1}, and a full barb is 10 m s^{-1}. The black line in (b) highlights the shortwave trough.

b. *Storm reports and damage indicators*

Hail reports in Fig. 1 are taken from the public Storm Report[2] database, managed by the PRETEMP team (De Martin et al. 2023). Since 2019, this database updates the European Severe Weather Database (Dotzek et al. 2009), representing the main source of reports for Italy. Besides hail reports, the PRETEMP team collected 1134 DIs of straight-line winds (486) and tornado (648) related to the Alfonsine event. These data were reported by several storm chasers and weather enthusiasts that conducted surveys in the hours following the event. Furthermore, other DIs were collected from satellite images provided by Microsoft Bing. Both downburst and tornado damage were rated with the recently released IF scale (Groenemeijer et al. 2023). In the supplemental material, the complete list of reported damage indicators is provided. The DI list is divided into two files, one for the DIs related to the tornado (Table S1) and one for the DIs related to the straight-line wind (Table S2).

c. *Numerical simulations*

Operational simulations performed with version 4.5 of the Weather Research and Forecasting (WRF) Model (Skamarock et al. 2019) are used to assess the predictability of the event. These simulations use 38 vertical levels in a domain covering Italy with a horizontal grid spacing of 3.5 km. Simulations were initialized with initial and boundary conditions provided by Icosahedral Nonhydrostatic–Europe (ICON-EU) (6.5-km grid spacing; Reinert et al. 2020), a nest of the global simulations made by ICON (13.5-km grid spacing; Zängl et al. 2015) over Europe. The physics configuration of the model is set with the Yonsei University PBL scheme (Hong et al. 2006), the Rapid Radiative Transfer Model for GCMs (RRTMG) for longwave radiation (Iacono et al. 2008), the Dudhia (1989) scheme for shortwave radiation, Ferrier-ETA for microphysics, the Revised Monin–Obukhov Similarity scheme (Jiménez et al. 2012) for surface-layer physics, and the Noah land surface model (Mukul Tewari et al. 2004). No cumulus scheme is used.

The simulations are initialized every 6 h before the event, and they are integrated out to 72 h. The first simulation is initialized at 1800 UTC 19 July 2023, and the others subsequently at 6-h intervals. A total of 12 simulations are considered. The average cumulative rainfall and maximum updraft helicity simulated in the 1200 UTC 22 July 2023–1800 UTC 22 July 2023 are computed as a function of the lead time using 24-h windows. Hence, three means are obtained considering: the simulations initialized 72, 66, 60, and 54 h ahead (up to 3 days in advance); those initialized 48, 42, 36, and 30 h ahead (up to 2 days in advance); and those initialized 24, 18, 12, and 6 h ahead (up to 1 day in advance). These means are used to assess whether the model was able to simulate the development of supercells in the afternoon of 22 July 2023 in the area affected by the damaging downburst and tornado.

3. Results

a. *Synoptic analysis*

On 22 July 2023, a subtropical ridge was located in the southern Mediterranean region (Fig. 2a). An intense zonal flow was present in the northern Mediterranean region, with the peak wind speed over the Ligurian Sea at 200 hPa (55 m s^{-1}; Fig. 2a). An upper-level shortwave trough traversed northern Italy on this day, as can be inferred from the weak cyclonic curvature of the geopotential heights at 500 hPa and the relative humidity gradient at 700 hPa (identified by the black line in Fig. 2b). A

[2] https://www.meteonetwork.it/tt/stormreport/.

weak cyclonic curvature is appreciable also at 700 hPa over the Alps. In the low-levels, there was no significant advection of cold air, suggesting that a well-defined cold front was not crossing the region, in agreement with the synoptic analysis of the Met Office.[3]

b. Mesoscale dynamics

At 1200 UTC 22 July 2023, a very moist easterly flow from the Adriatic Sea was present in the eastern part of the Emilia-Romagna region (Fig. 3a), associated with high values of dewpoint temperature (T_d). This is a known key feature for severe storm development in northern Italy since it provides moisture along with latent instability (Manzato et al. 2015; Miglietta et al. 2016; Bagaglini et al. 2021; De Martin et al. 2024).

At 1100 UTC, a sounding was launched inside the high-T_d tongue in San Pietro Capofiume (black dot in Fig. 3a), 2 h before the tornado occurrence and 30 km northwest of Alfonsine. Thus, this sounding can be considered representative of the prestorm environment. The sounding-derived parameters (Fig. 4) are compared with the climatology of ERA5 proximity soundings of F2–F3 tornadoes in Europe obtained by Taszarek et al. (2020b) in the 1979–2018 period. The mixed-layer (ML, using the layer between surface and 500 m AGL) convective available potential energy (CAPE) was much higher than the 90th percentile observed during F2–F3 tornado events in Europe (2786 J kg^{-1} vs about 1400 J kg^{-1}). Similarly, ML CAPE 0–3 km, i.e., ML CAPE in the first 3 km of the troposphere, a very useful proxy for tornadogenesis (Rasmussen 2003; Thompson et al. 2003), was as high as the 90th percentile (130 J kg^{-1}). Additionally, the lifting condensation level (LCL) was fairly low (1065 m), and the lapse rate in the 0–3-km layer (7.8 K km^{-1}) was above the 90th percentile for F2–F3 tornado events. Mid- and deep-layer shear were strong as well, thanks to the intense west-southwest flow shown earlier in the synoptic maps: the bulk shear in the 0–6-km layer was 27.9 m s^{-1}, and the 0–3-km storm-relative helicity (SRH) was equal to 171 m^2 s^{-2}. Consequently, there was a very favorable overlap of latent instability, mid- and deep-layer wind shear, low LCL, and steep lapse rates for tornadic supercells. However, the bulk shear in the 0–1-km layer (5.8 m s^{-1}) was significantly lower than the mean value for European F2–F3 tornado events (about 10 m s^{-1}), and the hodograph was straight. The presence of low values of SRH during tornado events in the Po Valley was already observed by Bagaglini et al. (2021) and De Martin et al. (2024). However, using the observed storm motion (retrieved by tracking the maximum of SRI in Fig. 3 between 1200 and 1315 UTC) to compute the SRH, values of 326 m^2 s^{-2} in the 0–3-km layer and of 102 m^2 s^{-2} in the 0–1-km layer are obtained. Hence, the storm turned right more than what was expected from the Bunkers formula (Bunkers et al. 2000; 53° to the right instead of 26°), likely because it was following the boundary of the moist air advected from the sea (Fig. 3) and because of the strong pressure perturbations (Fig. 5), as suggested by Bunkers (2018). Consequently, the storm-relative helicity experienced by that specific storm was much higher. Furthermore, while surface winds were weak in the location where the sounding was launched, observations to the east near the Adriatic coast suggest a stronger easterly flow was present at the surface when the storm occurred (Fig. 3b). In section 3e, we show evidence that this proximity sounding underestimated the low-level helicity the storm locally experienced. The vertical profile was rather favorable also for straight-line wind occurrence, due to the presence of the strong midlevel flow, the high precipitable water (41 mm), the strong gradient of Θ_e between the surface and midlevels (Atkins and Wakimoto 1991), and the dry air intrusion above 500 hPa (Miglietta et al. 2025).

An isolated storm developed in the western plain of the Lombardy region at about 0800 UTC (see the radar animation Video S1), and it moved first eastward and then southeastward toward the Emilia-Romagna region (storm 1 in Fig. 1). It produced hail that did not exceed 5 cm in diameter in Lombardy.

A second isolated storm was triggered further south, in the Apennine foothills in the Emilia-Romagna region at 1130 UTC (Fig. 3a, storm in Fig. 1). Consequently, two isolated storms were present in or nearby the Emilia-Romagna region at 1200 UTC: both were supercells since they had a deviant motion with respect to the synoptic westerly flow (see Video S1), a persistent hook echo (Fig. 6a), and a bounded weak echo region (ARPAE 2013). A similar situation with two intense simultaneous supercells in the Emilia-Romagna region was observed on 18 June 1997 (Alberoni et al. 2000) and on 3 May 2013 (ARPAE 2013). The two storms moved eastward approaching the moist easterly flow from the Adriatic Sea (Fig. 3b), progressively intensifying, as can be inferred from the hail sizes reported in Fig. 1, and, regarding storm 1, also from the deepening of the mesocyclone's pressure drop, as recorded by the weather stations affected by its passage (Fig. 5a). However, storm 1 directly crossed the high-T_d tongue (Fig. 3), producing several reports of hailstones up to 10 cm wide (Fig. 1). On the other hand, storm 2 was marginally fed by the high-T_d tongue and produced smaller hailstones (only one report of an 8-cm-wide hailstone was collected), ultimately dissipating at 1400 UTC when it crossed a dry air mass in the lee of the Apennines (Fig. 3b).

Figure 6 shows the evolution of supercell 1 between 1215 and 1250 UTC at an elevation of approximately 2 km AGL, as observed from the radar of San Pietro Capofiume located at the black dot.[4] These images allow for a more precise determination of the storm-relative positions of weather stations B, C, and D. All stations were located within the inflow region, south of the hail core (the black triangle marks the location where a 10-cm-diameter hailstone was reported at 1240 UTC; note also the radar beam attenuation due to the hail core at 1240 UTC), and north of the hook echo. A progressive southward elongation of the hook echo is also evident. In particular, at 1250 UTC, the

[3] https://digital.nmla.metoffice.gov.uk/SO_3bf07d21-ae69-47f9-a293-23cc741a5a0d/.

[4] PPIs with increasing elevation angles are shown as the supercell approaches the radar site, in order to maintain a scanning height of approximately 2 km AGL within the hook echo. 1250 UTC is the last available time step before the radar was damaged by the storm.

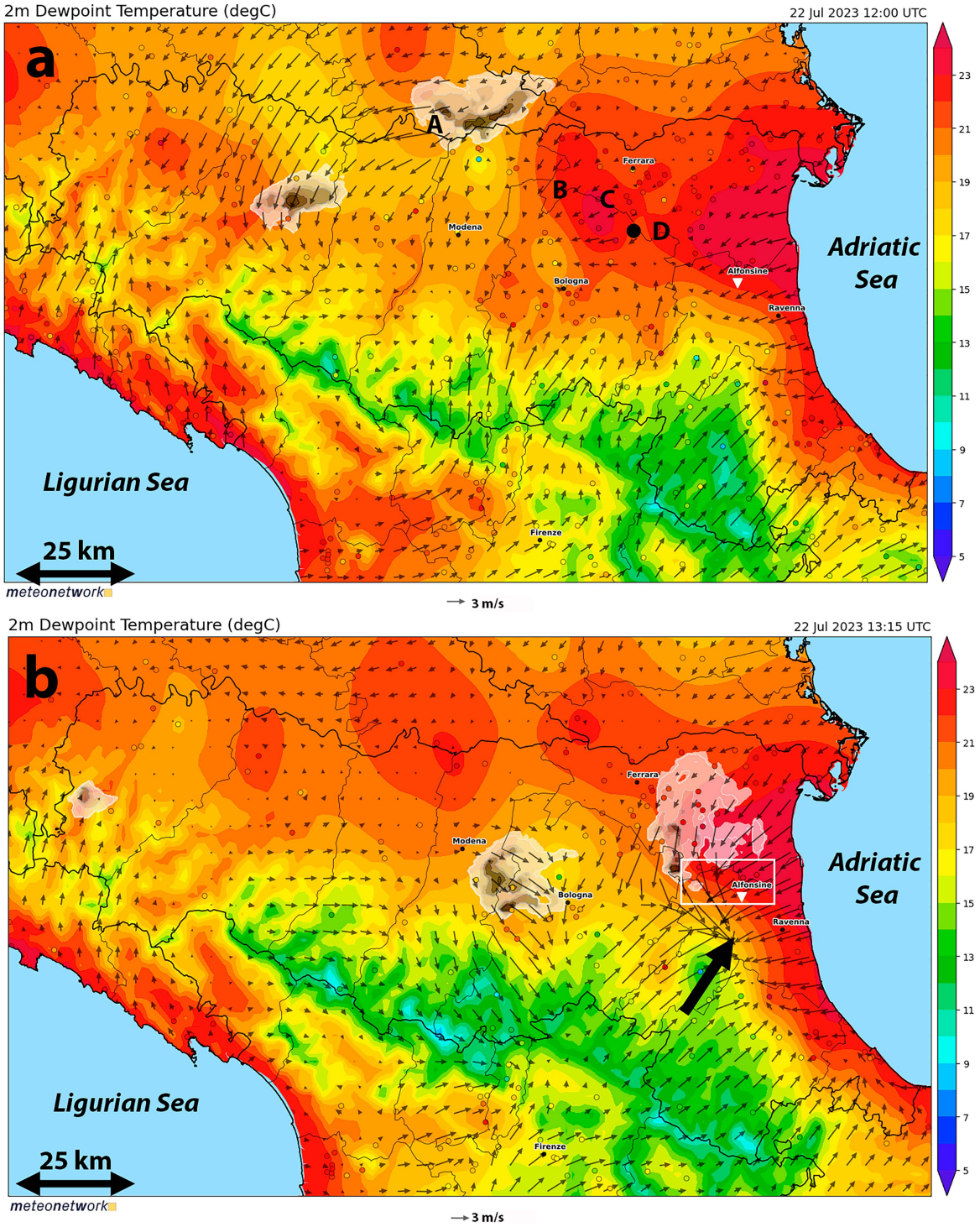

FIG. 3. (a) Interpolation with altitude correction (grid spacing 2.5 km) of dewpoint temperature (°C; color shading) and wind (arrows) measured by Meteonetwork weather stations (filled dots; color bar on the right) at 1200 UTC 22 Jul 2023. The gray shading represents values > 15 mm h^{-1} of SRI at 1200 UTC estimated by the national radar composite of the Civil Protection Department of Italy (darker values correspond to stronger intensity; contours for 15, 20, 50, 80, 100, and 150 mm h^{-1}). The domain is highlighted with the box in Fig. 1. A reference wind vector is provided at the bottom. Capital letters A, B, C, and D point out the locations of some of the weather stations analyzed in Fig. 5 (respectively the villages of Gonzaga, Dosso, Poggio Renatico, and Ospitalmonacale). The black dot in (a) indicates the location of the sounding shown in Fig. 4. (b) As in (a), but at 1315 UTC. The white box in (b) indicates the domain shown in Fig. 7a. The thick black arrow highlights the triple point location.

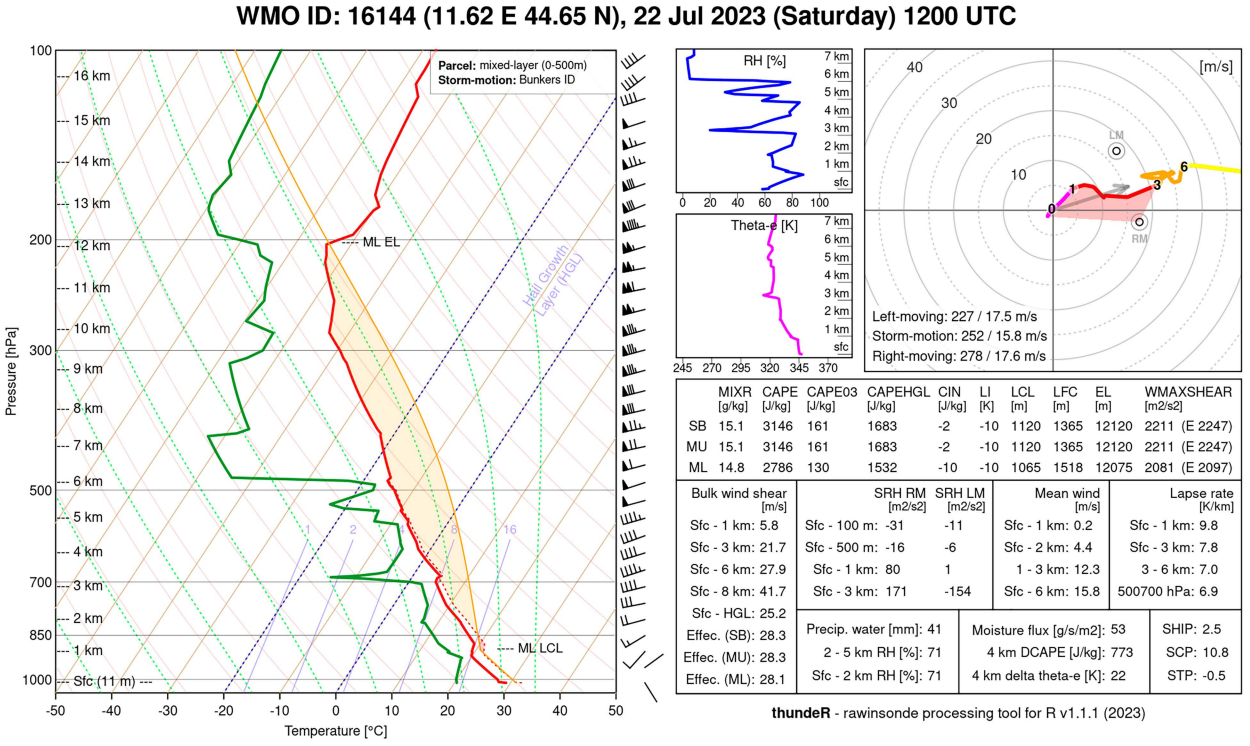

FIG. 4. Sounding launched at San Pietro Capofiume (location shown in Fig. 3a) at 1100 UTC 22 Jul 2023. Some relevant parameters are shown. The ML is computed for the first 500 m above ground level.

hook echo exhibits a more pronounced arching shape (black arrow in Fig. 6i) in the 2.3° PPI (approximately 300 m AGL), suggesting an imminent mesocyclone occlusion. Although no tornado damage was reported at that time, this feature clearly indicates the storm's tornadic potential.

At 1315 UTC, a dryline bulge is recognizable in Fig. 3b (thick black arrow): the very moist easterly flow from the Adriatic Sea converged with a dry southwesterly flow from the Apennines and with the outflows of the northern supercell. At that moment, the northern supercell generated an IF3 tornado close to Alfonsine. Significantly, the storm generated the tornado only when it encountered the dry air mass (and not before). The southern supercell that passed south of the dryline bulge did not generate a tornado.

c. *Tornado and downburst damage*

Initially, storm 1 produced damaging hail, but no wind damage was reported. Between 1245 and 1315 UTC, the hail size produced by the storm slightly decreased (from 10 to 7 cm), while the wind gusts were intensifying. Between 1500 and 1515 UTC, wind gusts up to 27.8 m s^{-1} were recorded in San Pietro Capofiume (location shown with a black dot in Fig. 6, ARPAE 2023). These gusts led to significant damage to the radar site and weather station. Some damage to buildings was reported 25 km west of Alfonsine (rated between IF0 and IF0.5).

At 1515 UTC, the supercell caused damage compatible with IF1 grade (about 40 m s^{-1}) in the town of Voltana di Lugo (Fig. 7): Multiple roofs were severely damaged, and trees were downed. After the analysis of the damage via ground and drone surveys,[5] as well as a few videos taken by local residents, the damage in this village appears to have been caused by at least two distinct microbursts (Fujita 1985): one affected the town from west-northwest (note the divergent wind pattern inside the white ellipse 1 in Fig. 7b; the same figure at the highest resolution is provided in Fig. S1) and the other from southwest (ellipse 2 in Fig. 7b). The two microbursts seem separated as no damage in between appears evident from satellite imagery. They may have converged toward a common center, where the first damage caused by a tornadic circulation was reported a few hundred meters east of the village. A similar pattern was noted and mapped after the 28 August 1990 Plainfield, Illinois, F5 tornado (Fig. 19 of Fujita 1993).

To further clarify the tornadogenesis process, in Fig. 8, satellite images taken after the event are shown for the area highlighted with a white dashed line in Fig. 7b. Two areas likely affected by microburst damage are shown in Fig. 8a: In Fig. 8b, some downed trees are visible, while in Fig. 8c, there are crops flattened by the wind. The wind causing that damage was unidirectional and slightly convergent. On the other hand, in Figs. 8d and 8e, some downed trees are visible in almost perpendicular directions.

The tornado moved eastward, affecting the small village of Chiesa Nuova with damages up to grade IF3. After having

[5] https://youtu.be/0ZbVacF7leM?si=atP4yEVeiWjZGrHy.

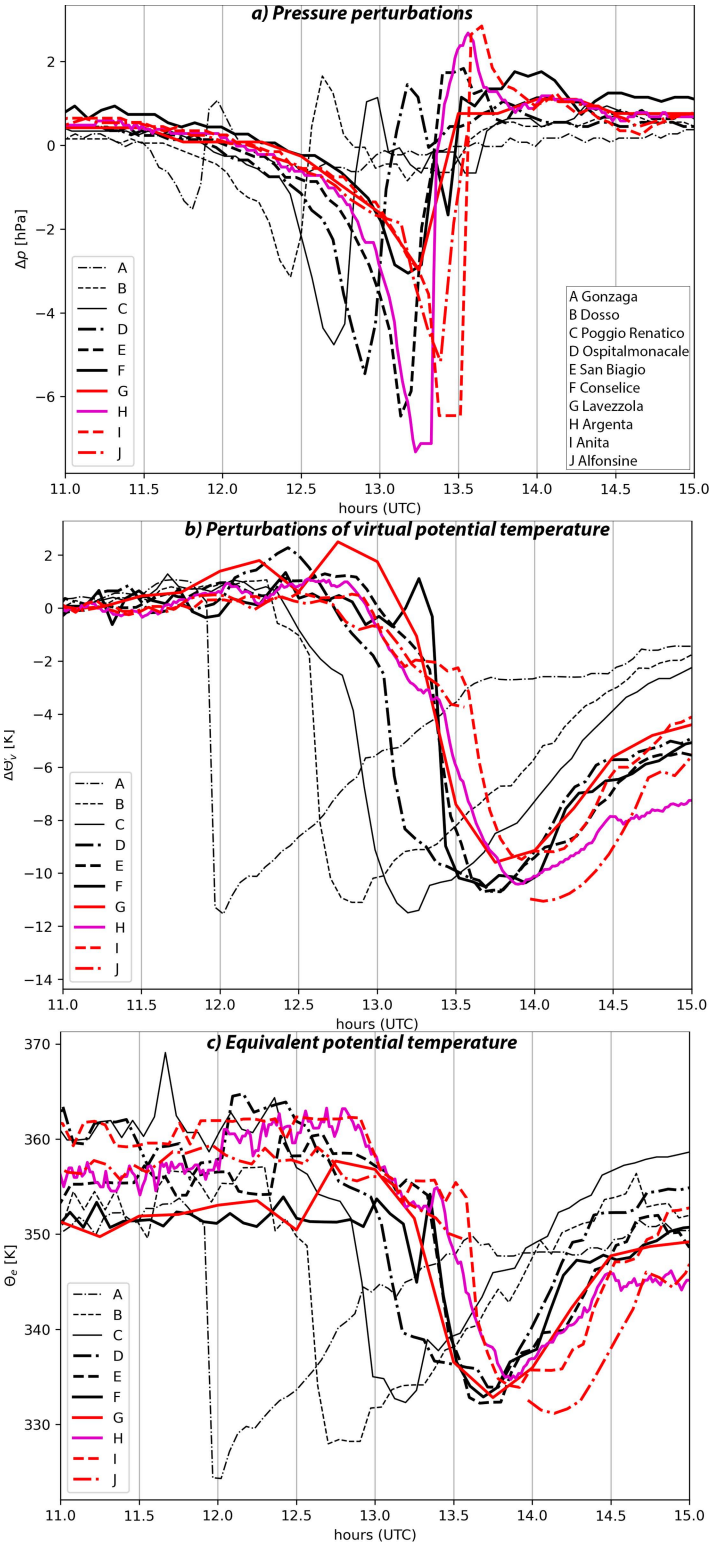

FIG. 5. (a) Pressure perturbations observed by weather stations located along the track of supercell 1 (locations shown in Figs. 3a and 7a); (b) as in (a), but for perturbations of virtual potential temperature; (c) as in (a), but for Θ_e values.

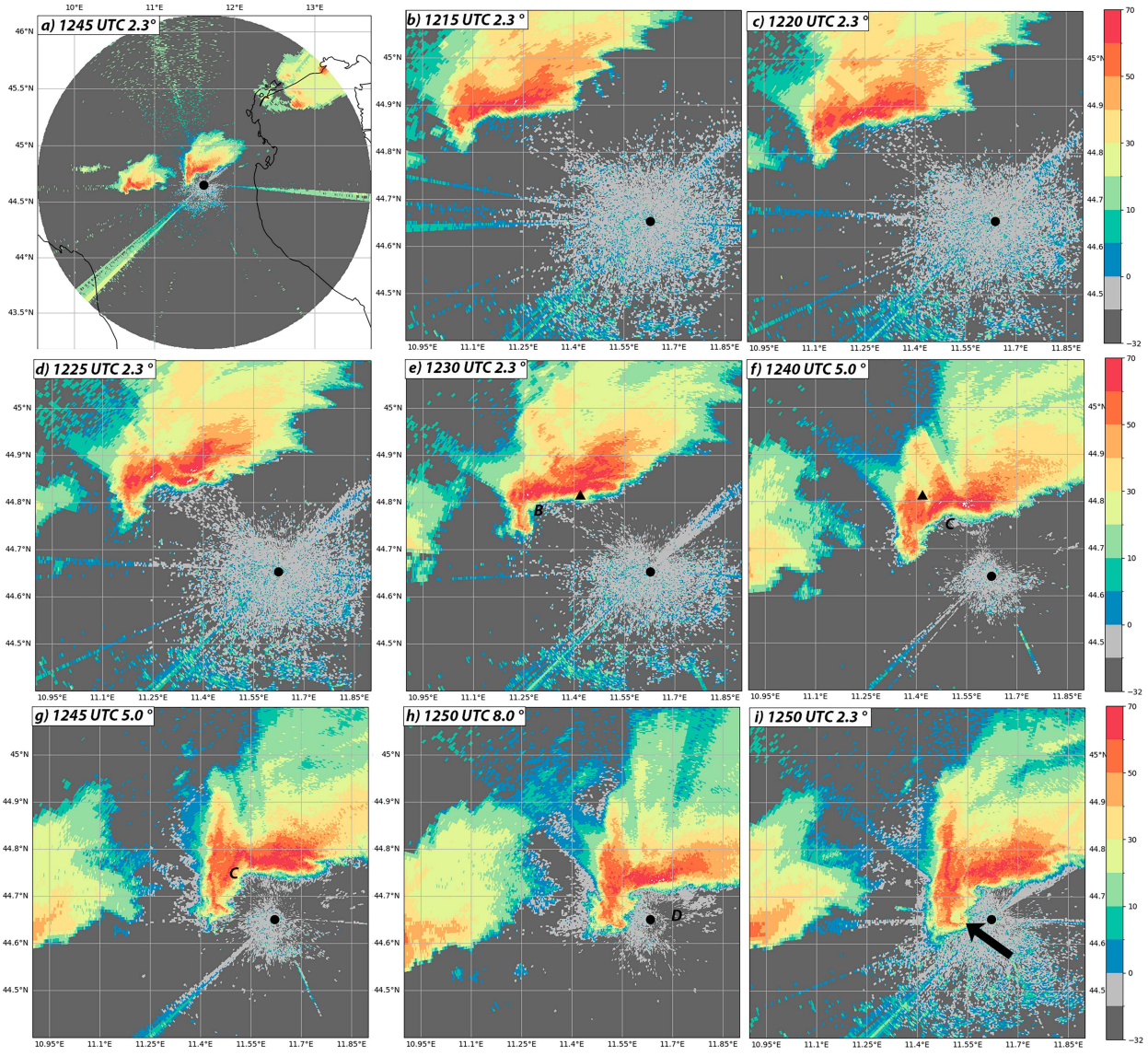

FIG. 6. (a) Reflectivity (color shading) measured by the San Pietro Capofiume radar (its location is marked with a black dot in both this panel and Fig. 3a) at a PPI scan with an elevation angle of 2.3° at 1245 UTC. Contours indicate coastlines. (b)–(e) As in (a), but at 1215, 1220, 1225, and 1230 UTC, respectively, and focused on a zoomed-in area. (f) As in (b), but at 1240 UTC and an elevation angle of 5.0°. (g) As in (f), but at 1245 UTC. (h) As in (g), but at an elevation angle of 8.0° and at 1250 UTC. (i) As in (h), but at an elevation angle of 2.3°. The black triangle in (e) and (f) marks the location where the largest hailstone was reported at 1240 UTC. Letters B, C, and D in (e)–(h) indicate the storm-relative positions of weather stations B, C, and D (see Fig. 3).

affected Taglio Corelli, the tornado deviated rightward (Fig. 7a). The change in direction of the tornado occurred when the RFD surge weakened: south of the tornado track, between Alfonsine and San Gregorio, there is a stripe without wind damage (Fig. 7a). A subvortex probably developed on the backside of the main vortex close to San Gregorio di Alfonsine. While the main vortex was moving east-southeastward generating damages up to grade IF3, a small area of curving IF1 to IF2.5 damage extended to the south (Fig. 7c). That damage path could be explained by a subvortex that was cyclonically turning around the main vortex; secondary tornadic circulations are typical of violent tornadoes (Wakimoto et al. 2016; Davies-Jones 2015). Then, the tornado moved north of Alfonsine for a few kilometers, affecting Borgo Seganti (other damages up to grade IF3), and finally it dissipated in the village of Savarna.

The microburst associated with the RFD dissipated a few kilometers west of the tornado, in correspondence of Alfonsine. There, the amateur weather station J (location shown in Fig. 7a) recorded a 5-s gust of 35.8 m s^{-1} from west-northwest at 1330 UTC (Randi 2024), 3 km southward of the tornado's path, which is in good agreement with the winds estimated

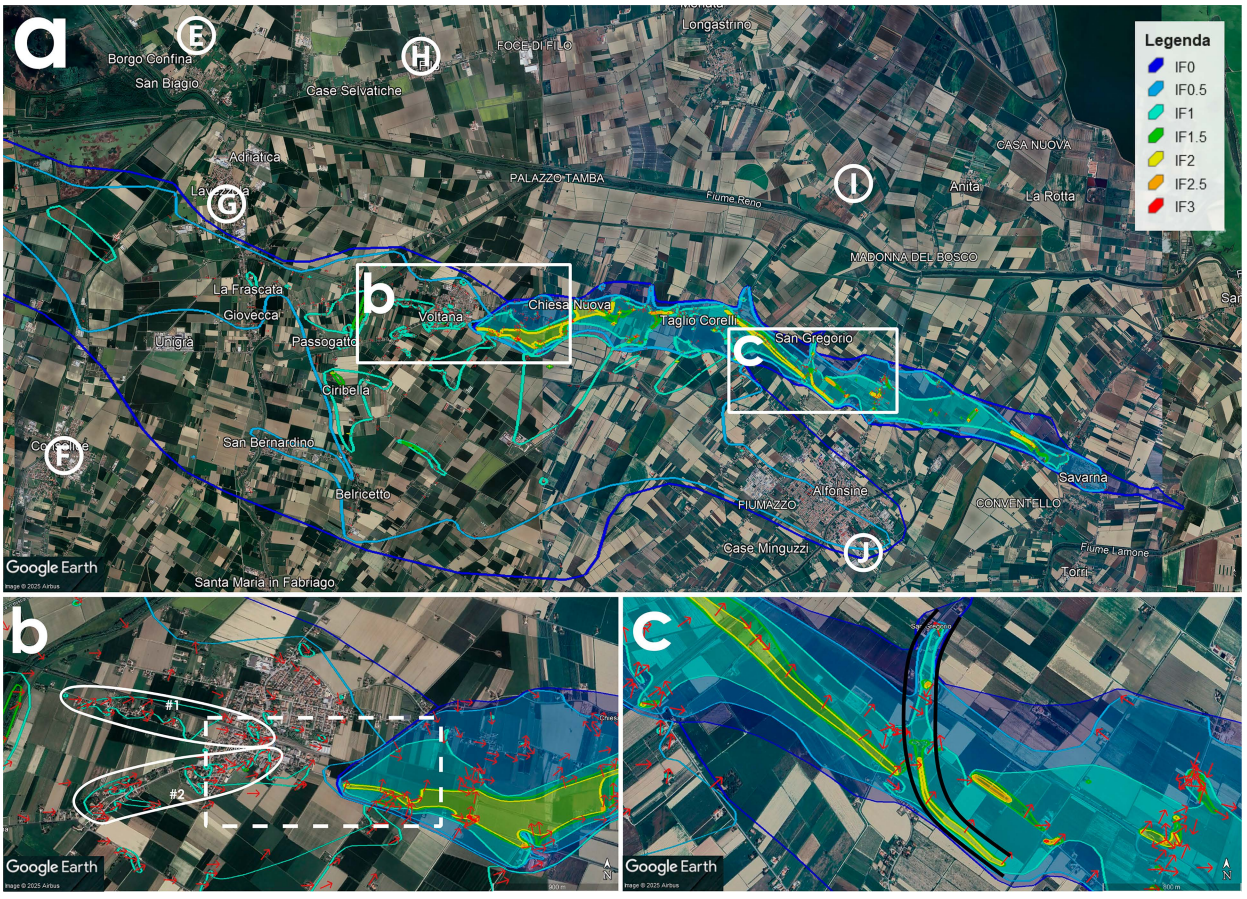

FIG. 7. (a) Damage reconstruction of the Alfonsine tornado (the plotted domain is indicated with a black box in Fig. 3b): Downburst damage is highlighted with contours, while tornado damage is highlighted with filled colors. Colors are referred to the IF scale: blue (IF0), turquoise green (IF0.5), green (IF1), light green (IF1.5), yellow (IF2), orange (IF2.5), and red (IF3) shading. DIs are reported in (a) as red arrows with directions according to the wind direction inferred from the damages (the same figure with much higher quality is provided in the supplemental material S1). Capital letters E, F, G, H, I, and J highlight the locations of the weather stations analyzed in Figs. 5 and 10. (b) Bottom-left inset, zoomed-in view of the damage pattern in Voltana di Lugo, where the tornado developed; (c) bottom-right inset, zoomed-in view of where a secondary vortex likely developed: Its path is highlighted with two black lines. Map data ©2024 Google.

from the observed damage in the town using the IF scale (IF1, ~40 m s^{-1}).

Analyzing the damage indicators, eight DIs (Fig. 9) out of a total of 648 tornadic DIs were rated as IF3. In Table 1, these indicators are described, following Tables 3 and 4 in Groenemeijer et al. (2023). This rating is consistent with an F3 rating using the Fujita scale (Fujita 1971). Overall, the tornado remained on the ground for about 16.7 km and reached a maximum width of 1.5 km (Fig. 7a).

d. Ground observations of tornadic supercell 1

The evolution of the mesocyclone and of the outflows can be determined from the data reported by the weather stations affected by storm 1 (identified by capital letters in Fig. 3a), in particular in the proximity of the tornado path (identified by capital letters in Fig. 7a).

As the mesocyclone of storm 1 intensified (greater pressure drop in Fig. 5a), the drop in Θ_v' associated with the storm outflows became slightly less pronounced (Fig. 5b). In fact, at 1200 UTC, Θ_v' dropped by −11.5 K at weather station A, whereas at weather station G, located 5 km west-northwest of the area where the first tornado damage was reported, Θ_v' decreased by −9.6 K at 1330 UTC (Fig. 5b). An exception was weather station J, situated 3 km south of the tornado track (Fig. 7a), which recorded a virtual potential temperature drop of −11.5 K. The observed drop in Θ_e was already remarkable at weather station A, generally around 20 K (Fig. 5c). Notably, just before the tornado occurred, weather stations E, H, I, and J (all positioned just north of the tornado path, Fig. 7a) recorded Θ_e values as high as 360 K (Fig. 5c) since the stations were within the high-T_d tongue (thus, it was also associated with high-Θ_e values). The minimum Θ_e observed after the passage of the storm increased over time, from 325 K at 1200 UTC to 333 K at 1330 UTC.

A comparison of Θ_e evolution at weather station H, located 5 km north of the tornado path, with the evolution of p' and

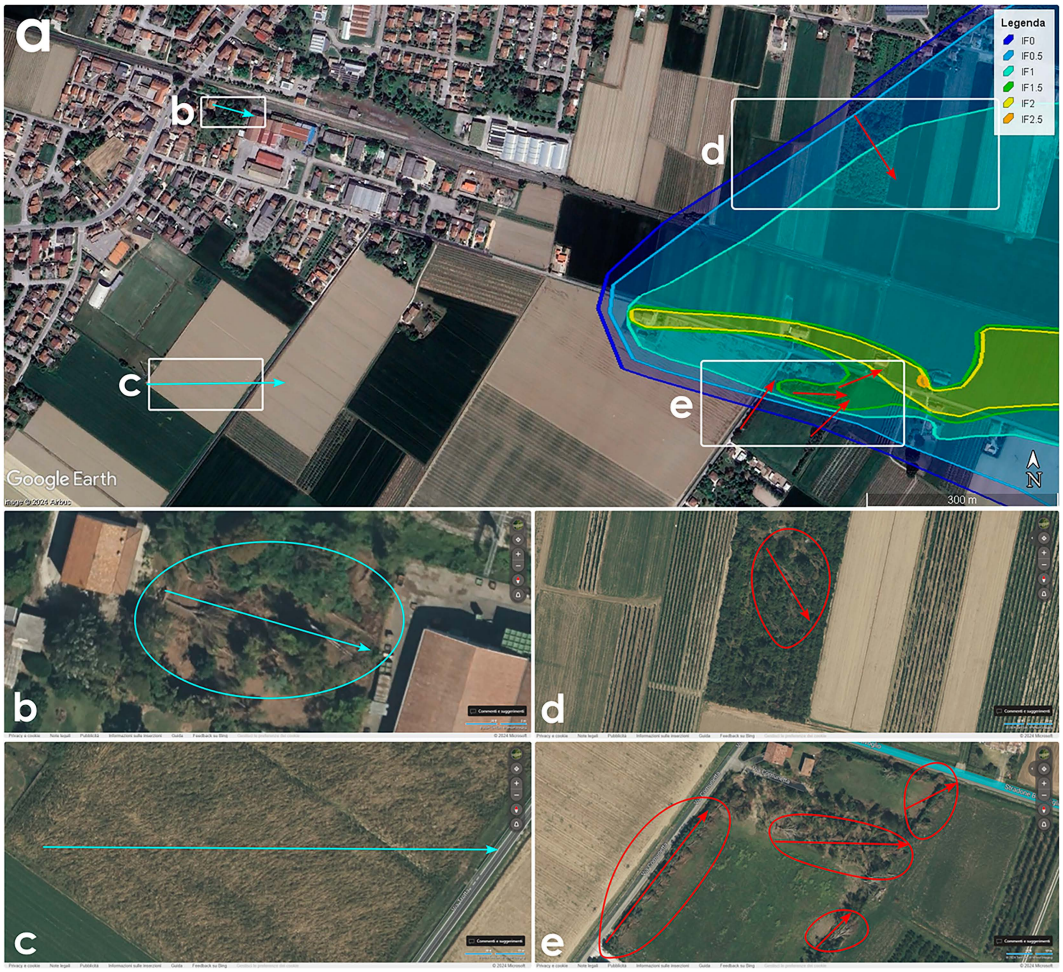

FIG. 8. (a) Satellite image taken a few days after the event showing the area highlighted with a dashed white box in Fig. 7b. The tornado damages are highlighted with color shading according to the IF scale as in Fig. 7. Blue (downburst) and red (tornado) arrows highlight the direction of the wind according to observed damage. Two areas affected by downburst damage and two areas affected by tornado damage are highlighted with white boxes and zoomed, respectively, in (b)–(e). Map data in (a) © 2024 Google. Images source in (b)–(e) are Microsoft (2023).

wind barbs is shown in Fig. 10a. At station H, pressure began to drop at 1200 UTC, while Θ_e values suddenly increased from 357 to 361 K, as the wind shifted from the north to the east-northeast. This suggests that, as the mesocyclone approached the site, it ingested the high-Θ_e air mass over the Adriatic Sea (Fig. 3). Just before the mesocyclone passage at 1315 UTC, the inflow blew at 11.1 m s^{-1} from the sea, with gusts reaching 17.7 m s^{-1}. Subsequently, the wind veered to the west before returning to the east-northeast, accompanied by a drop in Θ_e of more than 25 K within one hour. The pressure drop was −7.3 hPa, followed by an increase of about 10 hPa after the passage of the system. In Fig. 10b, the evolution of wind, 2-m temperature, T_d, Θ'_v, and p' in weather station F is shown. This weather station (that has a sample frequency of 5 min) was hit by the southern side of the mesocyclone. Notably, at 1309 UTC, the weather station recorded for just one time step a change of the wind from southeast to southwest, associated with an increase of temperature (from 31.5°C at 1259 UTC to 33.9°C) and a decrease of T_d (from 21.7°C at 1254 UTC to 17.6°C). Consequently, Θ'_v increased from −0.7 K at 1259 UTC to +1.1 K. This abrupt and brief change of air mass occurred just at the end of the drop of pressure caused by the mesocyclone, and just before the drop of Θ'_v caused by the RFD.

e. *Model simulations of tornadic supercell 1*

The simulation initialized at 1200 UTC 21 July 2023 (24 h before the event) reproduces the observed dryline (Fig. 3), even if in the simulation it is positioned a bit too far north (Fig. 11a). Its intensification between 1200 and 1300 UTC is also simulated (cf. Figures 11a,b). The presence of a very moist air mass over the Adriatic Sea is reproduced as well, associated with an easterly flow close to the Emilia-Romagna region coast. Furthermore, a supercell [see the updraft-helicity

FIG. 9. (a)–(h) Documented IF3 DIs caused by the Alfonsine tornado; pictures are by Gabriele Saviotti and Mattia Palombo in (a), (b), (d), Nicola Pirondini in (c), Mattia Palombo in (e) and (g), Dimitri Perchekliysky in (f), and Gianni Contessi in (h).

(UH) track in Fig. S3] is reproduced (Fig. 11b) just north of the dryline bulge at 1300 UTC as actually happened (Fig. 3b), making this simulation reliable.

The highest values of moisture near the ground are present along the surface boundaries and over the Adriatic Sea (Figs. 11a,b). Furthermore, SRH 0–1 km is generally weak (as pointed out by the sounding in Fig. 4), with the exceptions of the areas close to the boundaries, especially over the Adriatic coast along the dryline (SRH 0–1 km $\sim$ 150m^2 s^{-2}, Fig. 11c). Consequently, the highest values of the significant tornado parameter (STP $\sim$ 1, mean STP value for F2–F3 tornadoes in Europe is 0.4; Taszarek et al. 2020b) are located in a narrow

TABLE 1. Details for the IF3 rating of the DIs shown in Fig. 9.

DI photo	Damage indicator	Sturdiness class	Wall quality	Wall thickness (cm)	Degree of damage
Fig. 9a	Building structure	C	Unreinforced cast concrete	10–20	2 (near-complete destruction)
Fig. 9b	Building structure	D	Weak brick masonry	20–40	1B (partial destruction)
Fig. 9c	Building structure	C	Weak brick masonry	10–20	2 (near-complete destruction)
Fig. 9d	Building structure	C	Weak brick masonry	10–20	2 (near-complete destruction)
Fig. 9e	Building structure	E	Strong brick masonry	20–40	1A (some damage to structure)
Fig. 9f	Building structure	D	Weak brick masonry	20–40	1B (partial destruction)
Fig. 9g	Building structure	C	Unreinforced cast concrete	10–20	2 (near-complete destruction)
Fig. 9h	Building structure	C	Weak brick masonry	10–20	2 (near-complete destruction)

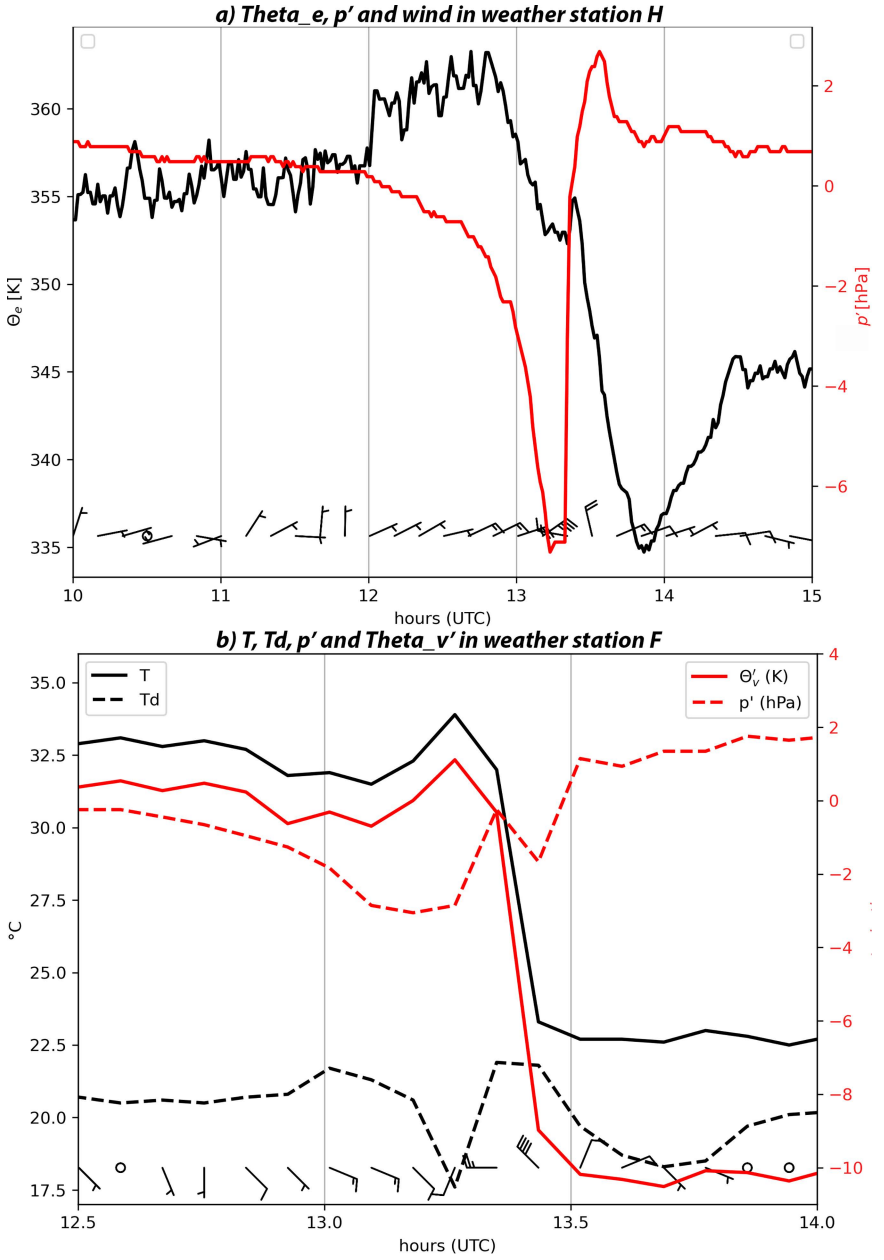

FIG. 10. (a) The Θ_e, pressure perturbations p', and wind sampled by weather station H (5 km north of the point where tornadogenesis occurred; location shown in Fig. 7a). (b) Temperature (T), dewpoint temperature (Td), Θ_v', and p' in weather station F (9 km west-southwest of the point where tornadogenesis occurred; location shown in Fig. 7a).

stripe along the Adriatic coast (Fig. 11e). Along the surface boundaries, there are also maxima of vertical vorticity (Fig. 11g). Ahead of the dryline, there are positive values of storm-relative streamwise vorticity (Fig. S4a).

As the supercell approaches the dryline bulge, the induced pressure perturbations (observed in Fig. 5a) intensify the easterly flow from the Adriatic Sea, increasing the moisture transport (Fig. 11b, as observed also in Fig. 10b), the surface storm-relative streamwise vorticity (Fig. S4b), the SRH 0–1 km close to the storm (Fig. 11d), and the STP that reaches values higher than 3 just east of the supercell (Fig. 11f). At the same time, downdrafts intensified due to the strong evaporative cooling at the midlevels (cross section AB in Fig. 11b is displayed in Fig. S5; Gilmore and Wicker 1998). Consequently, vertical vorticity maxima along the RFD boundary (Fig. 11h) deepen, likely due to the baroclinic downdraft mechanism (Parker and Dahl 2015). While at 1200 UTC, the environment does not appear supportive for significant tornadoes (weak SRH 0–1 km and STP), at 1300 UTC,

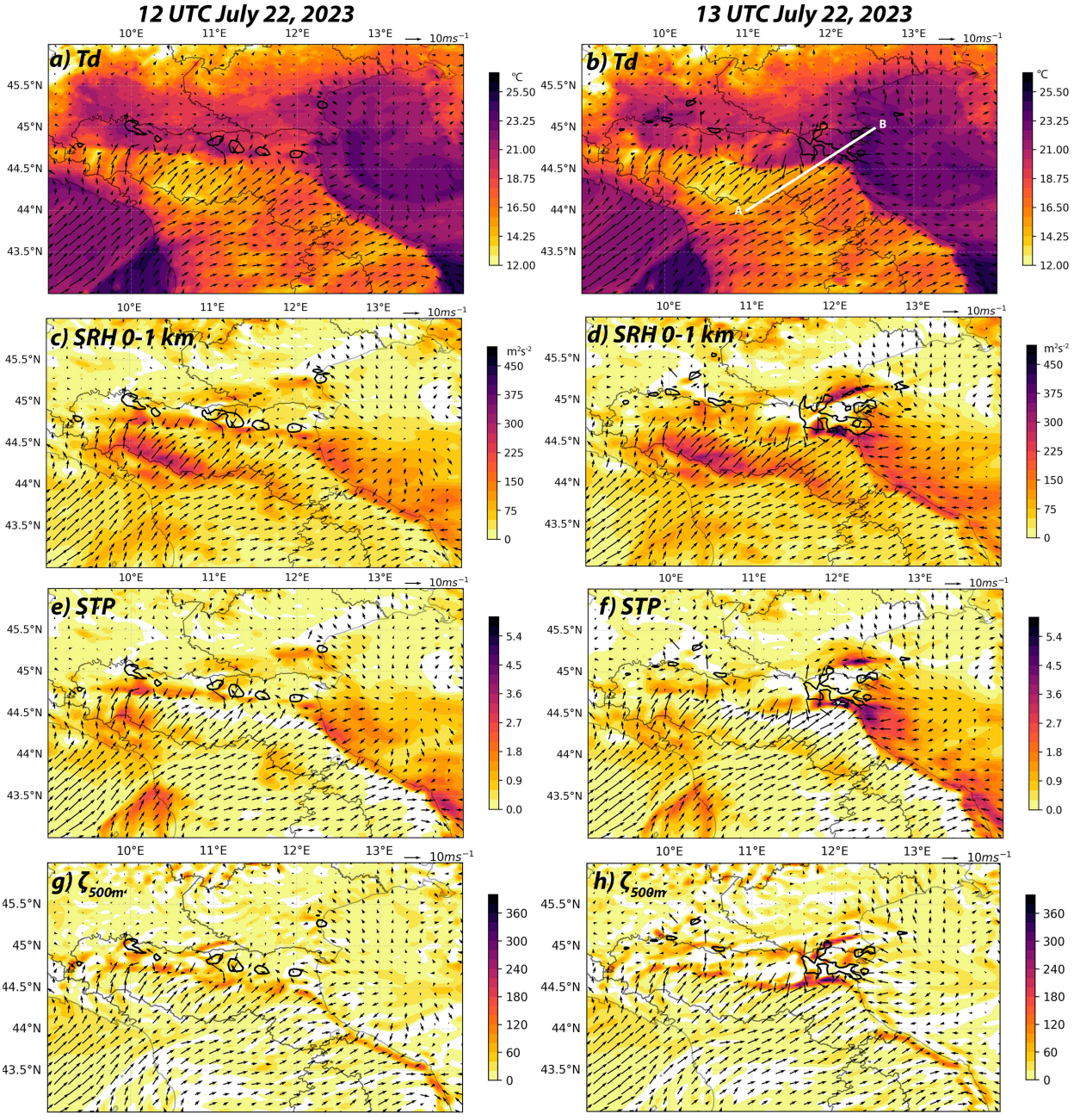

FIG. 11. (a) Dewpoint temperature (°C), (c) SRH 0–1 km (m^2 s^{-2}), (e) STP, and (g) vertical vorticity ζ at 500 m AGL (s^{-1}) at 1200 UTC 22 Jul 2024. (b),(d),(f),(h) As in (a), (c), (e), and (g), respectively, but at 1300 UTC 22 Jul 2023. In all the plots, wind speed at 10 m (arrows) and simulated reflectivity ≥ 30 dBZ at 1 km (black contours) are shown. Results of the WRF simulation initialized at 1200 UTC 21 Jul 2023.

the tornado potential is much higher. It appears the supercell may have at least partially enhanced its own ingredients for tornadogenesis as it encountered a more favorable environment.

To further clarify the source of the inflow ingested into the supercell along the dryline, we carry out a trajectory analysis at 1300 UTC using Visualization and Analysis Platform for Ocean, Atmosphere, and Solar Researchers (VAPOR ; UCAR/NCAR—Computational and Information System Lab 2023; Li et al. 2019). To this end, 30 seeds are released at 200 m AGL in the dry air mass, in the cold pool, and in the moist air mass over the Adriatic Sea (Fig. 12). Interestingly, Fig. 12 indicates that updraft trajectories originate in all three of the prominent air masses, including the warm, moist reservoir of the Adriatic, the hot, dry air mass behind the dryline, and the outflow region of the supercell. This numerical result is supported by the weather station F (Fig. 10b), which recorded a brief dry and hot airmass intrusion in the southern side of the mesocyclone at 1309 UTC. This result expands the findings of previous studies about supercells

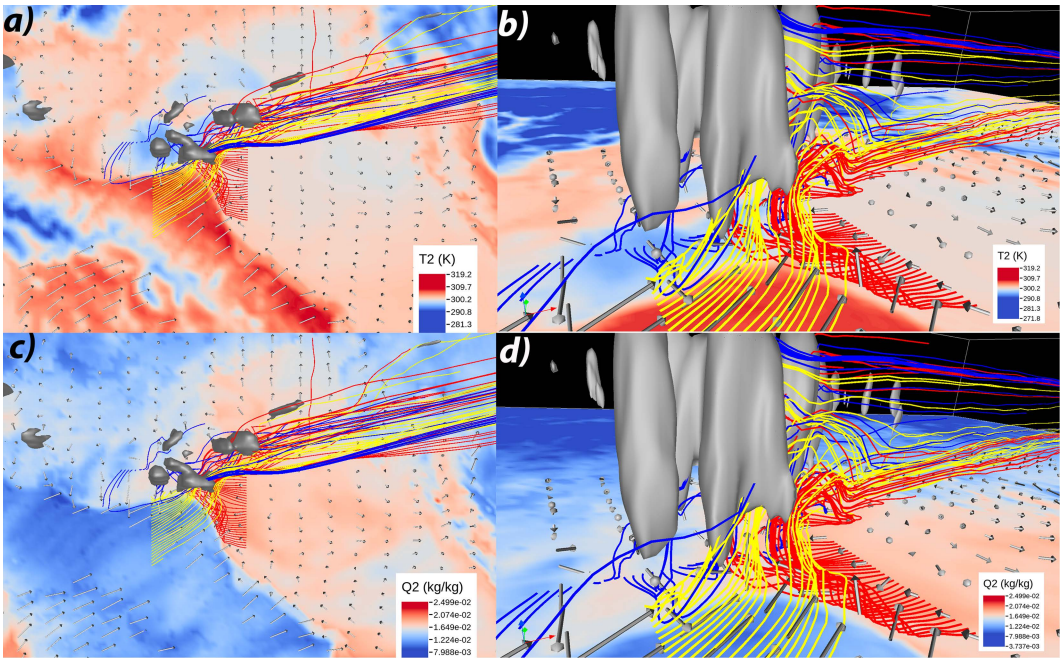

FIG. 12. (a) Temperature at 2 m (K; color shading), vertical velocity ≥ 7 m s^{-1} (gray patches), wind at 10 m (arrows), trajectories of 30 seeds released in the dry air mass (yellow lines), in the cold pools (blue lines), and in the moist maritime air mass (red lines). (c) As in (a), but with specific humidity (kg kg^{-1}) as color shading. (b),(d) As in (a) and (c), respectively, but with a three-dimensional view from the southwest.

along outflow boundaries (Atkins et al. 1999; Markowski et al. 1998). In this case, some of the hot and dry air behind the dryline is being ingested and mixed into the updraft.

f. Predictability of the event

After having clarified the peculiar dynamic evolution of the tornadic supercell, the severe storm predictability is briefly discussed using the operational WRF forecasts described in section 2c. Both mean cumulative precipitation and mean maximum UH in the 1200–1800 UTC period on 22 July 2023 are shown in Fig. 13. As early as three days in advance, the model was able to simulate convective storm precipitation tracks over northeastern Italy and a swath with UH values larger than 100 m^2 s^{-2} from the Emilia-Romagna region toward the Adriatic Sea, suggesting the potential for long-lived supercells. Approaching the event, the skill of the simulations slightly improved since the UH swath moved northward.

This set of simulations suggests that the predictability of the occurrence of supercells in the Emilia-Romagna region was quite high, considering that these forecasts are usually associated with large uncertainties in an area with complex topography (Miglietta et al. 2016). As early as three days in advance, a strong signal of the possible development of supercells can be detected in the Alfonsine area. Indeed, the Italian Civil Protection issued a yellow warning for local severe storms on 22 July 2023 in the Emilia-Romagna region[6] (i.e., general chances of localized damage). The predictability for tornado development is much more challenging to evaluate, and it is also intrinsically very low (Markowski 2020). However, given the quite high probability of long-lived supercells and the low LCLs (Bunkers et al. 2006; Markowski et al. 2002), PRETEMP mentioned the possible occurrence of tornadoes in the area of Alfonsine in the outlook issued one day ahead.[7]

4. Discussion

A supercell (storm 1 in Fig. 1) developed in the Lombardy region, moving east-southeastward and intensifying (step 1 in Fig. 14a). It became a hail-bearing supercell upon crossing the Emilia-Romagna border, producing hailstones up to 10 cm in diameter (Fig. 1 and step 2 in Fig. 14a). The production of giant hailstones was likely favored by the strong mid- and upper-tropospheric flow, overlapping with sufficiently high values of latent instability [De Martin et al. (2025a) proposed that kinematic conditions were crucial for the development of giant hailstones in an Alpine area]. On the other hand, at that time, the environment was not supportive for strong tornadoes, given the lack of low-level wind shear (Figs. 11c,e).

As the storm moved toward the high-Θ_e tongue (Fig. 3), it strongly turned to the right (53° more than the mean storm motion obtained from the sounding), ingesting a higher amount of storm-relative helicity. Furthermore, latent instability increased,

[6] https://allertameteo.regione.emilia-romagna.it/singola-allerta/-/asset_publisher/FZPQSb6AzKtJ/Allerta-Bollettino/id/2308306.

[7] https://pretemp.altervista.org/archivio/2023/luglio/previsioni/22_07_2023.html.

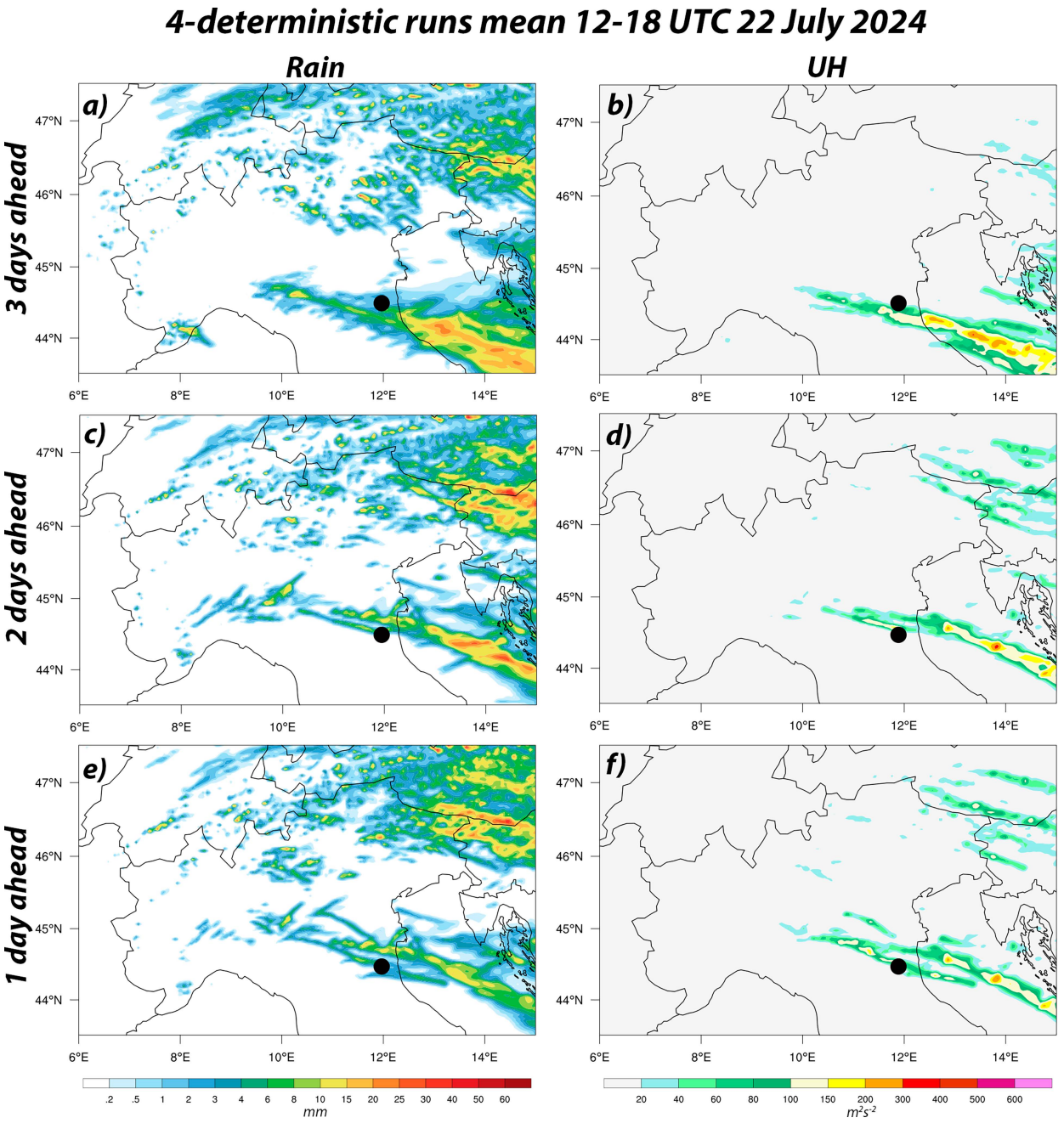

FIG. 13. (a) Mean cumulative rainfall at 1200–1800 UTC 22 Jul 2023 computed using the simulations initialized 72, 66, 60, and 54 h ahead (3 days ahead); (c) as in (a), but using simulations initialized 48, 42, 36, and 30 h ahead (2 days ahead); (e) as in (a), but using simulations initialized 24, 18, 12, and 6 h ahead (1 day ahead); (b),(d),(f) as in (a), (c), and (e), respectively, but for mean maximum UH. The black dot indicates the location of Alfonsine.

leading to stronger updrafts and a deepening of the mesocyclone, as suggested by the increasing magnitude of the observed pressure perturbations (Fig. 5a). With the mesocyclone intensifying, the stronger pressure perturbations progressively enhanced the RFD surge (step 3 in Fig. 14a; Skinner et al. 2014; Markowski et al. 2018). The RFD surge began causing wind damage 25 km west of Alfonsine, while hail size started decreasing. Along the RFD gust front, significant vertical vorticity was produced (Fig. 11h). The absolute values of the drops in Θ_v' and Θ_e (Figs. 5b,c) were much greater than those observed for tornadic supercells during field campaigns in the United States (e.g., VORTEX; Markowski et al. 2002; Shabbott and Markowski 2006). While such extreme values were caused by a midtropospheric dry intrusion (Fig. S4), the

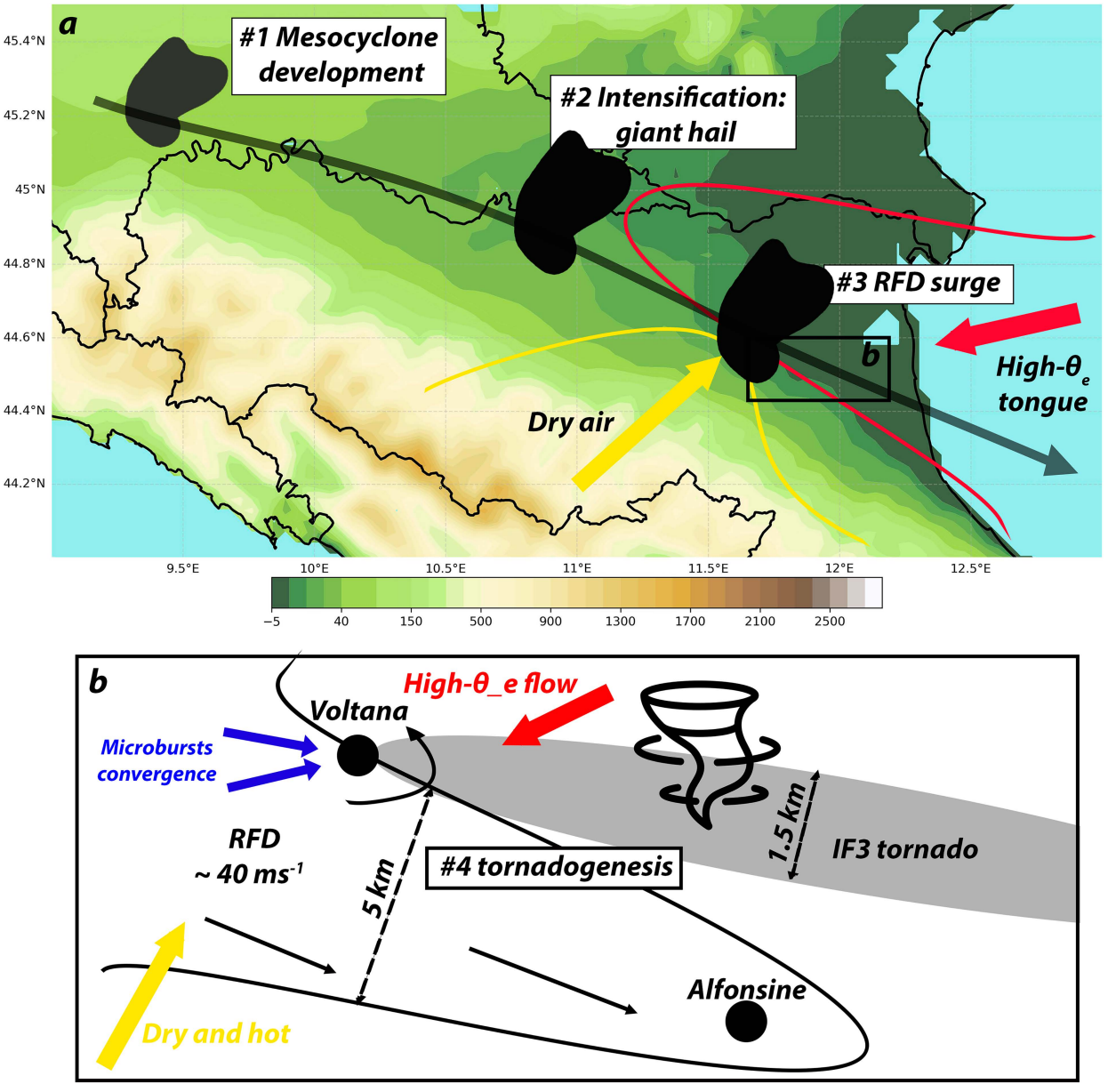

FIG. 14. Conceptual model of the Alfonsine tornado event: (a) three stages of the supercell evolution in the Emilia-Romagna region (colors represent topographic height); (b) a sketch of the tornadogenesis process that occurred within the black box in (a).

drop in Θ_v' and Θ_e associated with the downdraft slightly decreased from 1200 to 1315 UTC (Figs. 5b,c), suggesting that evaporative cooling was not intensifying or that the inflow was becoming warmer.

When the supercell approached the dryline bulge, it ingested both the high-Θ_e air mass over the Adriatic Sea (Figs. 5c and 11b) and the dry and hot air mass from the southwest, as seen in both data recorded by a weather station in the southern side of the mesocyclone (Fig. 10b) and the numerical simulation (Fig. 12). A similar situation was noted during the tornadic outbreak that occurred in central Europe in 1967 (Antonescu et al. 2020), with a tornadic supercell presenting a dry sector on the same side as the one studied in the present article (Wessels 1968).

In Voltana, two distinct microbursts converged (Fig. 7b), and the worst damage caused by the RFD gusts (~40 m s^{-1}) was reported. The intense RFD gusts possibly produced vertical vorticity patches (stage b in Fischer et al. 2024). The seamless wind damage pattern, from damage caused by straight-wind gusts to tornadic damage, supports the hypothesis that the tornado developed from the stretching of small-scale pretornadic vertical vorticity maxima within the RFD (Parker 2023). Potentially, the increase roughness of the village favored the tornadogenesis process, increased surface drag, and favored

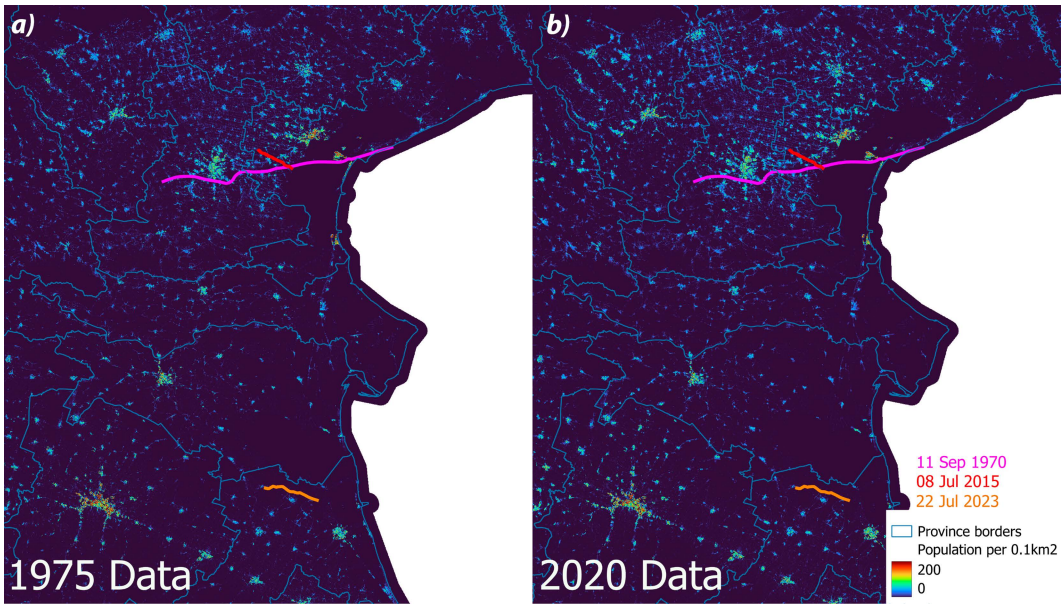

FIG. 15. Population density in (a) 1975 and (b) 2020 in the eastern Po Valley. Source: Commission (2024). The tracks of the Alfonsine (orange line), Dolo–Mira (red line), and Padua–Venice (purple line) tornadoes are reported.

the in-and-up mechanism (Houser et al. 2025; Fischer et al. 2024).

The dynamics of this significant tornadic supercell are consistent with the conceptual model described in De Martin et al. (2024). However, in the present study, we conducted a more in-depth analysis of the storm-scale processes, providing greater clarity on the peculiar local environment in which the tornado developed. Moreover, the previous study suggested that the baroclinic generation of streamwise vorticity along an outflow boundary may have favored tornadogenesis. In our case, no evident mesoscale outflow boundary was present; therefore, we believe that the baroclinic process played only a marginal role.

The Alfonsine tornado was the strongest tornado in Italy since the Mira–Dolo tornado on 8 July 2015 (ESSL 2015). While the tornado's pathlength and intensity were significant, northern Italy has experienced even longer-lasting and stronger tornadoes in the twentieth century, such as the Padua–Venice tornado on 11 September 1970 (Janeselli 1972). Notably, the Alfonsine tornado was the widest tornado documented in the Po Valley to date, although unverified reports exist of tornadoes up to 2 km wide on 4 July 1965, in the Emilia-Romagna region (as reported by newspapers *Libertà* and *L'Avvenire*, 6 July 1965).

The area affected by both the tornado and the RFD surge was particularly large (Fig. 7). However, only 14 injuries were reported. The tornado impacted a sparsely populated area (137 inhabitants per square kilometer in 2020), and the IF3 damage was restricted to uninhabited buildings (Fig. 9), while villages were generally spared (Fig. 7). As a result, the limited exposure of the area helped contain the number of injuries.

The Po Valley is one of the most densely populated regions in Europe. The previously mentioned tornadoes in 1970 and 2015 (Fig. 15) struck areas with significantly higher population densities (785 and 616 inhabitants per square kilometer, respectively, Table 2). The 1970 tornado caused 36 fatalities and at least 245 injuries along a 69.8-km path with a peak intensity

TABLE 2. Metadata of three remarkable tornadoes in northeastern Italy. Population density (source: Commission 2024) was computed considering a 6-km-wide box, centered in correspondence of the center of the tornado track. Economic losses were retrieved from newspaper articles.

	11 Sep 1970 Padua–Venice	8 Jul 2015 Dolo–Mira	22 Jul 2023 Alfonsine
Rating	F4	IF4	IF3
Fatalities	36	1	0
Injuries	245+	72	14
Economic losses (€)	N/A	100,000,000	101,600,000
Average width (m)	450	700	890
Max width (m)	N/A	1000	1500
Pathlength (km)	69.8	12.3	16.8
1975 population density (inhabitants per square kilometer)	785	616	115
2020 population density (inhabitants per square kilometer)	877	676	137

of F4. The more recent IF4 tornado in Dolo–Mira in 2015 resulted in 1 fatality and 72 injuries, in spite of a relatively modest pathlength of 12.3 km. Population density in the region continues to rise. In the area affected by the 1970 tornado, the population density increased from 785 inhabitants per square kilometer in 1970 to 877 inhabitants per square kilometer in 2020 (Table 2). Moreover, during summer, the beaches along the northern Adriatic coast are crowded with tourists, and large outdoor events are common.

While exposure to tornado risk is growing, vulnerability remains largely unchanged between 1970 and 2023. Despite the ability of the Italian Civil Protection to issue general thunderstorm warnings, tornado-specific warnings are not officially provided. Most of the population is unaware of proper tornado safety procedures—for example, some people during the Alfonsine tornado were injured because they remained inside their vehicles.[8] Additionally, tornado shelters are nonexistent. If a tornado similar to the 1970 Venice–Padua event were to occur today in the same area, it could result in a catastrophe. A similar conclusion was reached by Antonescu et al. (2018) with respect to the tornado risk in central Europe. Moreover, Strader et al. (2024) found that in the U.S. southern plains, tornado impact potential has increased by 50% since 1980 due to urban expansion, despite a slight decrease in tornado frequency.

The rarity of significant tornadoes in Italy should not limit the lack of preparedness by public authorities. The Alfonsine event demonstrates that a reliable severe storm warning indicating the potential for tornadic supercells could have been issued at least one day in advance (Fig. 13), as also indicated by the PRETEMP outlook. Additionally, the progressive intensification of the supercell on 22 July 2023, as it moved toward Alfonsine—where a dryline bulge was present (Figs. 3 and 6)—could have been used to pinpoint the area with the highest tornado potential a few minutes before the tornadogenesis.

5. Conclusions

A dense network of weather stations, a nearby sounding site, and weather radar, along with surveys carried out by many weather amateurs, allowed for a detailed reconstruction of the IF3 Alfonsine tornadic supercell's evolution and of the vortex's damage path, providing an unprecedented level of detail in Italy and with very few precedents in Europe. This multiobservational analysis showed that the tornadic supercell developed in an atmospheric environment highly conducive to supercell formation, characterized by high latent instability (significantly higher than in other violent European tornadoes; Pilguj et al. 2022) and strong midtropospheric wind shear, while modest regional values of low-level storm-relative helicity limited tornado development. Initially, the supercell produced giant hailstones (up to 10 cm in diameter) and an intense and strongly negative buoyant RFD, likely due to the evaporative cooling caused by a midtropospheric dry intrusion. The tornado was likely the result of four main factors. First, the long duration of the supercell permitted a progressive deepening of the mesocyclone, which led to the formation of an intense RFD surge. Second, the ingestion of the highly moist and buoyant air mass from the sea likely further strengthened the low-level updraft and mesocyclone. Third, the dryline was a source of enhanced low-level streamwise and vertical vorticity. Fourth, the strong deviant motion, possibly caused by the strong pressure perturbations and by the presence of the surface boundary, determined the ingestion of a higher amount of storm-relative helicity for this specific storm.

Last, this study highlighted that Italy remains unprepared for major tornado events, with an increasing exposure to tornado risk over northeastern Italy. To address these issues, the following measures should be considered:

1) Residents of northeastern Italy must be educated about tornado risks. They should be familiar with appropriate safety measures and learn how to interpret tornado outlooks and warnings.
2) This study confirms that the Alfonsine tornado did not occur unexpectedly. A tornado outlook issued one day in advance could have been feasible, and its implementation within the Italian Civil Protection system is strongly encouraged.
3) A nowcasting-based tornado warning system could also be effective. Currently, in Italy, nowcasting of precipitation is carried out by regional weather services and by the Department of Civil Protection; however, it is not specifically aimed at detecting supercells and tornadoes (e.g., radial velocities are not used). Radar data, soundings, weather station observations, and reports from storm spotters (as has been done in the United States for decades through the Skywarn program; Doswell et al. 1999) could be used to identify areas with the highest tornado potential. The IT-Alert system, which utilizes cell broadcast technology and was introduced by the EU Directive 2018/1972, could serve as a starting point for tornado warnings in Italy.
4) Building regulations should be updated to account for the potential impact of tornadic winds. While Italian buildings are generally more resistant to strong winds than their American counterparts, no specific tornado shelters currently exist. In certain settings (e.g., outdoor event venues, beaches, sports facilities), the implementation of tornado shelters should be considered, especially in the most exposed regions.

Further research should focus to better understand the effect of the ingestion of a near-ground dry and hot air mass in a tornadic supercell, as observed in this case study. A hypothesis that should be tested with idealized numerical simulations is that the dry and hot air mass may have diluted the excessively cold RFD where the tornadogenesis occurred. The resulting air mass may have possessed a higher Θ_v' and greater buoyancy, favoring its uplift by the mesocyclone and the stretching of the vorticity patches. Another possibility that should be investigated is that the gusty, dry, and hot southwesterly flow may have created streaks of vertical vorticity

[8] https://www.today.it/cronaca/tornado-ravenna-14-feriti-due-colpiti-da-alberi-caduti.html.

that may have served as focal points for tornadogenesis, as recently suggested by Markowski (2024) in a simulation with a turbulent boundary layer.

Acknowledgments. Rich Rotunno is acknowledged for fruitful discussions about this case study. Agostino Manzato is acknowledged for preliminary discussions about this event. Chris Broyles, Pieter Groenemeijer, and an anonymous reviewer are acknowledged for their insightful comments and revisions of this article. Storm spotters of the Storm Report project are gratefully acknowledged. Alessio Ceragioli, Samuele Montedero, Mattia Palombo, Nicola Pirondini, Gabriele Saviotti, Pierluigi Randi, Luca Tecchiato, and Federico Zandona are acknowledged for the damage surveys carried out. Radarmeteo is acknowledged for sharing the WRF Model outputs with the PRETEMP team. MMM acknowledge financial support from Next Generation EU, Mission 4, Component 1, CUP B53D23007360006, project "Thunderstorm outflows measurements and modeling for strong WIND nowcast and RISK mitigation (WIND RISK)."

Data availability statement. Ground observations, provided by Meteonetwork association, are available through the open-data web portal Mistral (https://meteohub.mistralportal.it/app/datasets); sounding plots and data are available at https://www.rawinsonde.com/thunder_app/; ERA5 reanalysis data are available through the Copernicus Climate Data Store (https://cds.climate.copernicus.eu); storm reports are available through the Storm Report database (https://www.meteonetwork.it/tt/stormreport/). Population data are taken from Commission (2024). WRF simulation output and radar data are too big to be publicly archived with available resources; data are archived locally and are available upon request to the corresponding author.

REFERENCES

Alberoni, P. P., V. Levizzani, R. J. Watson, A. R. Holt, S. Costa, P. Mezzasalma, and S. Nanni, 2000: The 18 June 1997 companion supercells: Multiparametric Doppler radar analysis. *Meteor. Atmos. Phys.*, **75**, 101–120, https://doi.org/10.1007/s007030070018.

Antonescu, B., D. M. Schultz, A. Holzer, and P. Groenemeijer, 2017: Tornadoes in Europe: An underestimated threat. *Bull. Amer. Meteor. Soc.*, **98**, 713–728, https://doi.org/10.1175/BAMS-D-16-0171.1.

——, J. G. Fairman Jr., and D. M. Schultz, 2018: What is the worst that could happen? Reexamining the 24–25 June 1967 tornado outbreak over western Europe. *Wea. Climate Soc.*, **10**, 323–340, https://doi.org/10.1175/WCAS-D-17-0076.1.

——, T. Púçik, and D. M. Schultz, 2020: Hindcasting the first tornado forecast in Europe: 25 June 1967. *Wea. Forecasting*, **35**, 417–436, https://doi.org/10.1175/WAF-D-19-0173.1.

ARPAE, 2013: Rapporto dell'evento meteorologico del 3 maggio 2013. Agenzia Regionale per la Protezione dell'Ambiente dell'Emilia Romagna Rep., 18 pp., https://www.arpae.it/it/temi-ambientali/meteo/report-meteo/rapporti-post-evento/rapporto-2013-12-dellevento-del-3-maggio-2013/view.

——, 2023: Rapporto dell'evento meteorologico del 22 luglio 2023. Agenzia regionale per la protezione dell'Ambiente dell'Emilia Romagna Rep., 28 pp., https://www.arpae.it/it/temi-ambientali/meteo/report-meteo/rapporti-post-evento/rapporto_meteo_20230722.pdf/view.

Atkins, N. T., and R. M. Wakimoto, 1991: Wet microburst activity over the southeastern United States: Implications for forecasting. *Wea. Forecasting*, **6**, 470–482, https://doi.org/10.1175/1520-0434(1991)006<0470:WMAOTS>2.0.CO;2.

——, M. L. Weisman, and L. J. Wicker, 1999: The influence of preexisting boundaries on supercell evolution. *Mon. Wea. Rev.*, **127**, 2910–2927, https://doi.org/10.1175/1520-0493(1999)127<2910:TIOPBO>2.0.CO;2.

Avolio, E., and M. M. Miglietta, 2022: Tornadoes in the Tyrrhenian regions of the Italian peninsula: The case study of 28 July 2019. *Atmos. Res.*, **278**, 106285, https://doi.org/10.1016/j.atmosres.2022.106285.

Bagaglini, L., R. Ingrosso, and M. M. Miglietta, 2021: Synoptic patterns and mesoscale precursors of Italian tornadoes. *Atmos. Res.*, **253**, 105503, https://doi.org/10.1016/j.atmosres.2021.105503.

Bech, J., R. Pascual, T. Rigo, N. Pineda, J. M. López, J. Arús, and M. Gayá, 2007: An observational study of the 7 September 2005 Barcelona tornado outbreak. *Nat. Hazards Earth Syst. Sci.*, **7**, 129–139, https://doi.org/10.5194/nhess-7-129-2007.

——, and Coauthors, 2011: A Mediterranean nocturnal heavy rainfall and tornadic event. Part I: Overview, damage survey and radar analysis. *Atmos. Res.*, **100**, 621–637, https://doi.org/10.1016/j.atmosres.2010.12.024.

Bechini, R., D. Giaiotti, A. Manzato, F. Stel, and S. Micheletti, 2001: The June 4th 1999 severe weather episode in San Quirino, Italy: A tornado event? *Atmos. Res.*, **56**, 213–232, https://doi.org/10.1016/S0169-8095(00)00074-0.

Bertato, M., D. B. Giaiotti, A. Manzato, and F. Stel, 2003: An interesting case of tornado in Friuli-northeastern Italy. *Atmos. Res.*, **67–68**, 3–21, https://doi.org/10.1016/S0169-8095(03)00043-7.

Bunkers, M. J., 2018: Observations of right-moving supercell motion forecast errors. *Wea. Forecasting*, **33**, 145–159, https://doi.org/10.1175/WAF-D-17-0133.1.

——, B. A. Klimowski, J. W. Zeitler, R. L. Thompson, and M. L. Weisman, 2000: Predicting supercell motion using a new hodograph technique. *Wea. Forecasting*, **15**, 61–79, https://doi.org/10.1175/1520-0434(2000)015<0061:PSMUAN>2.0.CO;2.

——, M. R. Hjelmfelt, and P. L. Smith, 2006: An observational examination of long-lived supercells. Part I: Characteristics, evolution, and demise. *Wea. Forecasting*, **21**, 673–688, https://doi.org/10.1175/WAF949.1.

Chmielewski, T., H. Nowak, and K. Walkowiak, 2013: Tornado in Poland of August 15, 2008: Results of post-disaster investigation. *J. Wind Eng. Ind. Aerodyn.*, **118**, 54–60, https://doi.org/10.1016/j.jweia.2013.04.007.

Coffer, B. E., M. Taszarek, and M. D. Parker, 2020: Near-ground wind profiles of tornadic and nontornadic environments in the United States and Europe from ERA5 reanalyses. *Wea. Forecasting*, **35**, 2621–2638, https://doi.org/10.1175/WAF-D-20-0153.1.

Commission, 2024: GHSL data package 2023. JRC Scientific Information Systems and databases Rep., European Commission, 95 pp., https://doi.org/10.2760/098587.

Czernecki, B., M. Taszarek, and P. Szuster, 2022: thundeR - Computation and Visualisation of Atmospheric Convective Parameters. R Package, https://bczernecki.github.io/thundeR/.

Davies-Jones, R., 2015: A review of supercell and tornado dynamics. *Atmos. Res.*, **158–159**, 274–291, https://doi.org/10.1016/j.atmosres.2014.04.007.

De Martin, F., and Coauthors, 2023: Toward a dedicated warning system of severe storms in Italy: The PRETEMP project. *11th European Conf. on Severe Storms*, Bucharest, Romania, European Severe Storms Laboratory, https://doi.org/10.5194/ecss2023-18.

——, S. Davolio, M. M. Miglietta, and V. Levizzani, 2024: A conceptual model for the development of tornadoes in the complex orography of the Po Valley. *Mon. Wea. Rev.*, **152**, 1357–1377, https://doi.org/10.1175/MWR-D-23-0222.1.

——, A. Manzato, N. Carlon, M. Setvák, and M. M. Miglietta, 2025a: Dynamic and statistical analysis of giant hail environments in northeast Italy. *Quart. J. Roy. Meteor. Soc.*, **151**, e4945, https://doi.org/10.1002/qj.4945.

——, M. M. Miglietta, T. Gastaldo, M. Martinazzo, F. Pavan, M. Siena, and S. Di Sabatino, 2025b: The Bayesian sinking in Porticello: A predictable convective windstorm? *Weather*, https://doi.org/10.1002/wea.7715, in press.

Doswell, C. A., III, 2003: Societal impacts of severe thunderstorms and tornadoes: Lessons learned and implications for Europe. *Atmos. Res.*, **67–68**, 135–152, https://doi.org/10.1016/S0169-8095(03)00048-6.

——, A. R. Moller, and H. E. Brooks, 1999: Storm spotting and public awareness since the first tornado forecasts of 1948. *Wea. Forecasting*, **14**, 544–557, https://doi.org/10.1175/1520-0434(1999)014<0544:SSAPAS>2.0.CO;2.

Dotzek, N., 2003: An updated estimate of tornado occurrence in Europe. *Atmos. Res.*, **67–68**, 153–161, https://doi.org/10.1016/S0169-8095(03)00049-8.

——, P. Groenemeijer, B. Feuerstein, and A. M. Holzer, 2009: Overview of ESSL's severe convective storms research using the European Severe Weather Database ESWD. *Atmos. Res.*, **93**, 575–586, https://doi.org/10.1016/j.atmosres.2008.10.020.

Dudhia, J., 1989: Numerical study of convection observed during the winter monsoon experiment using a mesoscale two-dimensional model. *J. Atmos. Sci.*, **46**, 3077–3107, https://doi.org/10.1175/1520-0469(1989)046<3077:NSOCOD>2.0.CO;2.

ESSL, 2015: Corporate report on the 8 July 2015 tornado of Mira (VE), Italy. European Severe Storm Laboratory Rep., 7 pp., https://www.essl.org/cms/wp-content/uploads/20150902-Mira-Tornado-of-8-July-2015-Report.pdf.

Fischer, J., J. M. L. Dahl, B. E. Coffer, J. L. Houser, P. M. Markowski, M. D. Parker, C. C. Weiss, and A. Schueth, 2024: Supercell tornadogenesis: Recent progress in our state of understanding. *Bull. Amer. Meteor. Soc.*, **105**, E1084–E1097, https://doi.org/10.1175/BAMS-D-23-0031.1.

——, and Coauthors, 2025: Invited perspectives: Thunderstorm intensification from mountains to plains. *Nat. Hazards Earth Syst. Sci.*, **25**, 2629–2656, https://doi.org/10.5194/nhess-25-2629-2025.

Fujita, T. T., 1971: Proposed mechanism of suction spots accompanied by tornado. *Seventh Conf. On Severe Local Storms*, Kansas City, Missouri, Amer. Meteor. Soc., 208–213, https://cir.nii.ac.jp/crid/1570291224905026560.

——, 1985: *The Downburst.* Satellite and Mesometeorology Research Project, Department of the Geophysical Sciences, University of Chicago, 122 pp.

——, 1993: Plainfield tornado of August 28, 1990. *The Tornado: Its Structure, Dynamics, Prediction, and Hazards*, *Geophys. Monogr.*, Vol. **79**, Amer. Geophys. Union, 1–17, https://doi.org/10.1029/GM079p0001.

Giaiotti, D. B., and F. Stel, 2007: A multiscale observational case study of an isolated tornadic supercell. *Atmos. Res.*, **83**, 152–161, https://doi.org/10.1016/j.atmosres.2005.08.007.

Giazzi, M., and Coauthors, 2022: Meteonetwork: An open crowd-sourced weather data system. *Atmosphere*, **13**, 928, https://doi.org/10.3390/atmos13060928.

Gilmore, M. S., and L. J. Wicker, 1998: The influence of midtropospheric dryness on supercell morphology and evolution. *Mon. Wea. Rev.*, **126**, 943–958, https://doi.org/10.1175/1520-0493(1998)126<0943:TIOMDO>2.0.CO;2.

Groenemeijer, P., and T. Kühne, 2014: A climatology of tornadoes in Europe: Results from the European Severe Weather Database. *Mon. Wea. Rev.*, **142**, 4775–4790, https://doi.org/10.1175/MWR-D-14-00107.1.

——, and Coauthors, 2023: The International Fujita (IF) scale. 78 pp., https://www.essl.org/cms/wp-content/uploads/IF-scale_v1.0c.pdf.

Groenemeijer, P. H., and A. van Delden, 2007: Sounding-derived parameters associated with large hail and tornadoes in the Netherlands. *Atmos. Res.*, **83**, 473–487, https://doi.org/10.1016/j.atmosres.2005.08.006.

Hannesen, R., N. Dotzek, and J. Handwerker, 2000: Radar analysis of a tornado over hilly terrain on 23 July 1996. *Phys. Chem. Earth.*, **25B**, 1079–1084, https://doi.org/10.1016/S1464-1909(00)00156-8.

Hersbach, H., and Coauthors, 2020: The ERA5 global reanalysis. *Quart. J. Roy. Meteor. Soc.*, **146**, 1999–2049, https://doi.org/10.1002/qj.3803.

Holzer, A. M., T. M. E. Schreiner, and T. Púčik, 2018: A forensic re-analysis of one of the deadliest European tornadoes. *Nat. Hazards Earth Syst. Sci.*, **18**, 1555–1565, https://doi.org/10.5194/nhess-18-1555-2018.

Homar, V., M. Gayà, R. Romero, C. Ramis, and S. Alonso, 2003: Tornadoes over complex terrain: An analysis of the 28th August 1999 tornadic event in eastern Spain. *Atmos. Res.*, **67–68**, 301–317, https://doi.org/10.1016/S0169-8095(03)00064-4.

Hong, S.-Y., Y. Noh, and J. Dudhia, 2006: A new vertical diffusion package with an explicit treatment of entrainment processes. *Mon. Wea. Rev.*, **134**, 2318–2341, https://doi.org/10.1175/MWR3199.1.

Horton, S. L., 2024: Findings of tornado site investigations undertaken following damage during Storm *Ciarán* on 1–2 November 2023. *Weather*, **79**, 373–378, https://doi.org/10.1002/wea.7616.

Houser, J. B., J. Dang, and G. Yan, 2025: Investigating the effects of surface roughness on tornadoes using high-resolution numerical modeling. *105th AMS Annual Meeting*, New Orleans, LA, Amer. Meteor. Soc., 12–16, https://ui.adsabs.harvard.edu/abs/2025AMS...10555605H/abstract.

Iacono, M. J., J. S. Delamere, E. J. Mlawer, M. W. Shephard, S. A. Clough, and W. D. Collins, 2008: Radiative forcing by long-lived greenhouse gases: Calculations with the AER radiative transfer models. *J. Geophys. Res.*, **113**, D13103, https://doi.org/10.1029/2008JD009944.

Ingrosso, R., P. Lionello, M. M. Miglietta, and G. Salvadori, 2020: A statistical investigation of mesoscale precursors of significant tornadoes: The Italian case study. *Atmosphere*, **11**, 301, https://doi.org/10.3390/atmos11030301.

Janeselli, R., 1972: Il tornado che colpì la laguna di venezia i'11 settembre 1970 qualche considerazione intorno alla teoria elettrica dei tornado. 27 pp.

Jiménez, P. A., J. Dudhia, J. F. González-Rouco, J. Navarro, J. P. Montávez, and E. García-Bustamante, 2012: A revised scheme for the WRF surface layer formulation. *Mon. Wea. Rev.*, **140**, 898–918, https://doi.org/10.1175/MWR-D-11-00056.1.

Komjáti, K., Á. J. Varga, L. Méri, H. Breuer, and S. Kun, 2022: Investigation of a supercell merger leading to the EF4 tornado in the Czech Republic on June 24, 2021 using radar data and numerical model outputs. *Időjárás*, **126**, 457–480.

Lemon, L. R., A. Stan-Sion, C. Soci, and E. Cordoneanu, 2003: A strong, long-track, Romanian tornado. *Atmos. Res.*, **67–68**, 391–416, https://doi.org/10.1016/S0169-8095(03)00063-2.

Li, S., S. Jaroszynski, S. Pearse, L. Orf, and J. Clyne, 2019: VAPOR: A visualization package tailored to analyze simulation data in Earth system science. *Atmosphere*, **10**, 488, https://doi.org/10.3390/atmos10090488.

Longo, P., and A. Puppo, 1934: La tromba del 24 luglio 1930 nel territorio di treviso-udine. *Memorie del R. Ufficio Centrale di Meteorologia e Geofisica*, **4**, 5–68.

Manzato, A., S. Davolio, M. M. Miglietta, A. Pucillo, and M. Setvák, 2015: 12 September 2012: A supercell outbreak in NE Italy? *Atmos. Res.*, **153**, 98–118, https://doi.org/10.1016/j.atmosres.2014.07.019.

Markowski, P. M., 2020: What is the intrinsic predictability of tornadic supercell thunderstorms? *Mon. Wea. Rev.*, **148**, 3157–3180, https://doi.org/10.1175/MWR-D-20-0076.1.

——, 2024: A new pathway for tornadogenesis exposed by numerical simulations of supercells in turbulent environments. *J. Atmos. Sci.*, **81**, 481–518, https://doi.org/10.1175/JAS-D-23-0161.1.

——, E. N. Rasmussen, and J. M. Straka, 1998: The occurrence of tornadoes in supercells interacting with boundaries during VORTEX-95. *Wea. Forecasting*, **13**, 852–859, https://doi.org/10.1175/1520-0434(1998)013<0852:TOOTIS>2.0.CO;2.

——, J. M. Straka, and E. N. Rasmussen, 2002: Direct surface thermodynamic observations within the rear-flank downdrafts of nontornadic and tornadic supercells. *Mon. Wea. Rev.*, **130**, 1692–1721, https://doi.org/10.1175/1520-0493(2002)130<1692:DSTOWT>2.0.CO;2.

——, T. P. Hatlee, and Y. P. Richardson, 2018: Tornadogenesis in the 12 May 2010 supercell thunderstorm intercepted by VORTEX2 near Clinton, Oklahoma. *Mon. Wea. Rev.*, **146**, 3623–3650, https://doi.org/10.1175/MWR-D-18-0196.1.

Matsangouras, I. T., P. T. Nastos, H. B. Bluestein, and M. V. Sioutas, 2014: A climatology of tornadic activity over Greece based on historical records. *Int. J. Climatol.*, **34**, 2538–2555, https://doi.org/10.1002/joc.3857.

Microsoft, 2023: Bing maps. https://www.bing.com/maps?cp=44.538727%7E11.952781&lvl=13.7&style=h.

Miglietta, M. M., and R. Rotunno, 2016: An EF3 multivortex tornado over the Ionian region: Is it time for a dedicated warning system over Italy? *Bull. Amer. Meteor. Soc.*, **97**, 337–344, https://doi.org/10.1175/BAMS-D-14-00227.1.

——, and I. T. Matsangouras, 2018: An updated "climatology" of tornadoes and waterspouts in Italy. *Int. J. Climatol.*, **38**, 3667–3683, https://doi.org/10.1002/joc.5526.

——, A. Manzato, and R. Rotunno, 2016: Characteristics and predictability of a supercell during HyMeX SOP1. *Quart. J. Roy. Meteor. Soc.*, **142**, 2839–2853, https://doi.org/10.1002/qj.2872.

——, J. Mazon, and R. Rotunno, 2017: Numerical simulations of a tornadic supercell over the Mediterranean. *Wea. Forecasting*, **32**, 1209–1226, https://doi.org/10.1175/WAF-D-16-0223.1.

——, E. Avolio, C. L. Ciricugno, D. Conte, and M. Burlando, 2025: Environmental conditions favorable to the development of a wet downburst in a Mediterranean region. *Atmos. Res.*, **326**, 108304, https://doi.org/10.1016/j.atmosres.2025.108304.

Mukul Tewari, N., and Coauthors, 2004: Implementation and verification of the unified Noah land surface model in the WRF model (formerly paper number 17.5). *Proc. 20th Conf. on Weather Analysis and Forecasting/16th Conf. on Numerical Weather Prediction*, Seattle, WA, Amer. Meteor. Soc., 14.2a, https://ams.confex.com/ams/84Annual/techprogram/paper_69061.htm.

Parker, M. D., 2023: How well must surface vorticity be organized for tornadogenesis? *J. Atmos. Sci.*, **80**, 1433–1448, https://doi.org/10.1175/JAS-D-22-0195.1.

——, and J. M. L. Dahl, 2015: Production of near-surface vertical vorticity by idealized downdrafts. *Mon. Wea. Rev.*, **143**, 2795–2816, https://doi.org/10.1175/MWR-D-14-00310.1.

Pilguj, N., M. Taszarek, M. Kryza, and H. E. Brooks, 2022: Reconstruction of violent tornado environments in Europe: High-resolution dynamical downscaling of ERA5. *Geophys. Res. Lett.*, **49**, e2022GL098242, https://doi.org/10.1029/2022GL098242.

Púčik, T., P. Groenemeijer, D. Rỳva, and M. Kolář, 2015: Proximity soundings of severe and nonsevere thunderstorms in central Europe. *Mon. Wea. Rev.*, **143**, 4805–4821, https://doi.org/10.1175/MWR-D-15-0104.1.

——, and Coauthors, 2024: The violent tornado on 24 June 2021 in Czechia: Damage survey, societal impacts, and lessons learned. *Wea. Climate Soc.*, **16**, 411–429, https://doi.org/10.1175/WCAS-D-23-0080.1.

Randi, P., 2024: Analisi tornado sul ravennate del 22 luglio 2023. Rep., 57 pp., https://www.meteoprofessionisti.it/download/.

Rasmussen, E. N., 2003: Refined supercell and tornado forecast parameters. *Wea. Forecasting*, **18**, 530–535, https://doi.org/10.1175/1520-0434(2003)18<530:RSATFP>2.0.CO;2.

Rauhala, J., and D. M. Schultz, 2009: Severe thunderstorm and tornado warnings in Europe. *Atmos. Res.*, **93**, 369–380, https://doi.org/10.1016/j.atmosres.2008.09.026.

Reinert, D., and Coauthors, 2020: DWD database reference for the global and regional ICON and ICON-EPS forecasting system. DWD, 196 pp., https://www.dwd.de/DWD/forschung/nwv/fepub/icon_database_main.pdf.

Romero, R., M. Gayà, and C. A. Doswell III, 2007: European climatology of severe convective storm environmental parameters: A test for significant tornado events. *Atmos. Res.*, **83**, 389–404, https://doi.org/10.1016/j.atmosres.2005.06.011.

Rotunno, R., and H. B. Bluestein, 2024: Recent developments in tornado theory and observations. *Rep. Prog. Phys.*, **87**, 114801, https://doi.org/10.1088/1361-6633/ad7f6a.

Scheffknecht, P., S. Serafin, and V. Grubišić, 2017: A long-lived supercell over mountainous terrain. *Quart. J. Roy. Meteor. Soc.*, **143**, 2973–2986, https://doi.org/10.1002/qj.3127.

Shabbott, C. J., and P. M. Markowski, 2006: Surface in situ observations within the outflow of forward-flank downdrafts of supercell thunderstorms. *Mon. Wea. Rev.*, **134**, 1422–1441, https://doi.org/10.1175/MWR3131.1.

Skamarock, W. C., and Coauthors, 2019: A description of the Advanced Research WRF version 4. NCAR Tech. Note NCAR/TN-556+STR, 162 pp., https://www2.mmm.ucar.edu/wrf/users/docs/technote/v4_technote.pdf.

Skinner, P. S., C. C. Weiss, M. M. French, H. B. Bluestein, P. M. Markowski, and Y. P. Richardson, 2014: VORTEX2 observations of a low-level mesocyclone with multiple internal rear-flank downdraft momentum surges in the 18 May 2010 Dumas, Texas, supercell. *Mon. Wea. Rev.*, **142**, 2935–2960, https://doi.org/10.1175/MWR-D-13-00240.1.

Strader, S. M., V. A. Gensini, W. S. Ashley, and A. N. Wagner, 2024: Changes in tornado risk and societal vulnerability leading to greater tornado impact potential. *npj Nat. Hazards*, **1**, 20, https://doi.org/10.1038/s44304-024-00019-6.

Taszarek, M., and H. E. Brooks, 2015: Tornado climatology of Poland. *Mon. Wea. Rev.*, **143**, 702–717, https://doi.org/10.1175/MWR-D-14-00185.1.

——, ——, and B. Czernecki, 2017: Sounding-derived parameters associated with convective hazards in Europe. *Mon. Wea. Rev.*, **145**, 1511–1528, https://doi.org/10.1175/MWR-D-16-0384.1.

——, J. T. Allen, P. Groenemeijer, R. Edwards, H. E. Brooks, V. Chmielewski, and S.-E. Enno, 2020a: Severe convective storms across Europe and the United States. Part I: Climatology of lightning, large hail, severe wind, and tornadoes. *J. Climate*, **33**, 10 239–10 261, https://doi.org/10.1175/JCLI-D-20-0345.1.

——, ——, T. Púčik, K. A. Hoogewind, and H. E. Brooks, 2020b: Severe convective storms across Europe and the United States. Part II: ERA5 environments associated with lightning, large hail, severe wind, and tornadoes. *J. Climate*, **33**, 10 263–10 286, https://doi.org/10.1175/JCLI-D-20-0346.1.

Thompson, R. L., R. Edwards, J. A. Hart, K. L. Elmore, and P. Markowski, 2003: Close proximity soundings within supercell environments obtained from the rapid update cycle. *Wea. Forecasting*, **18**, 1243–1261, https://doi.org/10.1175/1520-0434(2003)018<1243:CPSWSE>2.0.CO;2.

UCAR/NCAR—Computational and Information System Lab, 2023: Visualization and analysis systems technologies. https://doi.org/10.5281/zenodo.7779648.

Wakimoto, R. M., and Coauthors, 2016: Aerial damage survey of the 2013 El Reno tornado combined with mobile radar data. *Mon. Wea. Rev.*, **144**, 1749–1776, https://doi.org/10.1175/MWR-D-15-0367.1.

Wesolek, E., and P. Mahieu, 2011: The F4 tornado of August 3, 2008, in northern France: Case study of a tornadic storm in a low CAPE environment. *Atmos. Res.*, **100**, 649–656, https://doi.org/10.1016/j.atmosres.2010.09.003.

Wessels, H. R. A., 1968: De zware windhozen van 25 Juni 1967. *Hemel Dampkring*, **66**, 155–177.

Zängl, G., D. Reinert, P. Rípodas, and M. Baldauf, 2015: The ICON (ICOsahedral non-hydrostatic) modelling framework of DWD and MPI-M: Description of the non-hydrostatic dynamical core. *Quart. J. Roy. Meteor. Soc.*, **141**, 563–579, https://doi.org/10.1002/qj.2378.

Zanini, M. A., L. Hofer, F. Faleschini, and C. Pellegrino, 2017: Building damage assessment after the *Riviera del Brenta* tornado, northeast Italy. *Nat. Hazards*, **86**, 1247–1273, https://doi.org/10.1007/s11069-017-2741-6.